*viruses*

MDPI

*Article*

# Three K2-Targeting *Sircambvirus* Phages: Evidence for Modular Evolution at Genome and Tailspike Levels

**Anna A. Vasilyeva *, Lydia I. Ilyenko, Maria V. Nesterova, George A. Skvortsov, Mikhail A. Yaitsky, Andrei V. Chaplin, Konstantin S. Troshin, Dmitriy A. Shagin, Natalia V. Orlova, Vyacheslav A. Kuzmenok and Peter V. Evseev ***

Pirogov Russian National Research Medical University, Ostrovityanova 1, 117997 Moscow, Russia; ilyenko_li@rsmu.ru (L.I.I.); mariallog5@gmail.com (M.V.N.); galaxy22242500@mail.ru (G.A.S.); yaitskiyma@gmail.com (M.A.Y.); okolomedik@gmail.com (A.V.C.); konstantinetr@gmail.com (K.S.T.); shagdim777@gmail.com (D.A.S.); vrach315@yandex.ru (N.V.O.); kuzmenok.vyacheslav@yandex.ru (V.A.K.)
* Correspondence: annavasilyeva.bioscience@gmail.com (A.A.V.); petevseev@gmail.com (P.V.E.)

**Abstract**

Three lytic bacteriophages, Kleo, Medik, and Spark, were isolated on K2-encapsulated *Klebsiella pneumoniae* and characterized experimentally and by comparative genomics. All three had contractile tails, formed haloed plaques, and were active against both K2 strains tested. On the KL13 isolate M190, Spark exhibited substantially higher plating efficiency (EOP = $1.75 \times 10^{-3}$), whereas Kleo and Medik showed only low-frequency plaque formation (EOP = $1.76 \times 10^{-8}$ and $2.78 \times 10^{-8}$, respectively). They exhibited rapid adsorption-associated declines in recoverable infectious phage titers and reduced preformed biofilm biomass by 59.6–75.8%, whereas survival outcomes in *Galleria mellonella* varied among phages and doses. Their 46.6–48.0-kb genomes represent candidate members of three distinct species within *Sircambvirus*. In a 452-genome dataset, gene-sharing relationships extended across whole-genome nucleotide clusters, while major capsid protein and large terminase ATPase-domain phylogenies partitioned the same proteomically coherent group of 54 *Jameshumphriesvirinae*-associated phages differently. Among the three isolates, whole-genome similarity was greatest between Medik and Spark, whereas the Kleo and Spark tailspike genes shared 99.60% nucleotide identity, compared with a median of 93.23% across the other 48 single-copy homologous genes. Tailspike N-terminal homologs were concentrated in *Jameshumphriesvirinae*-associated phages, whereas depolymerase-region homologs occurred across several families and tail morphotypes. Together, these patterns provide evidence for modular evolution at both genomic and intragenic levels.

**Keywords:** bacteriophage; *Klebsiella pneumoniae*; K2 capsular polysaccharide; *Sircambvirus*; *Jameshumphriesvirinae*; comparative genomics; phylogenomics; modular evolution; tailspike protein; capsule depolymerase

Check for updates

Academic Editor: Mikael Skurnik

Received: 8 October 2026
Revised: 12 November 2026
Accepted: 12 November 2026
Published: 17 November 2026

**Copyright:** © 2026 by the authors. Licensee MDPI, Basel, Switzerland. This article is an open access article distributed under the terms and conditions of the Creative Commons Attribution (CC BY) license.

## 1. Introduction

*Klebsiella pneumoniae* is a Gram-negative encapsulated bacterium of the family *Enterobacteriaceae* that can colonize the mucosal surfaces of the human gastrointestinal and upper respiratory tracts, but under certain conditions can cause severe extraintestinal infections. Clinically significant manifestations include pneumonia, urinary tract infections, wound and catheter-associated infections, bacteremia, sepsis, meningitis, and pyogenic liver abscesses [1]. A particular concern is the combination of virulence in specific clonal lineages with the high capacity of *K. pneumoniae* to acquire antibiotic resistance genes. In the updated

WHO bacterial priority pathogens list, carbapenem-resistant representatives of the order *Enterobacterales*, including *K. pneumoniae*, are classified among the pathogens for which the development of new antimicrobial strategies is particularly needed [2]. European surveillance data also indicate an unfavorable trend. According to the ECDC/EARS-Net report, in 2024, the estimated incidence of bloodstream infections caused by carbapenem-resistant *K. pneumoniae* (CRKP) was 3.51 cases per 100,000 population in the EU, exceeding the 2019 level by 61.0% and remaining above the target value set for 2030 [3]. The convergence of multidrug resistance (MDR) and increased virulence further complicates treatment.

The intraspecific diversity of *K. pneumoniae* is often considered through two partially overlapping pathotypes: classical *K. pneumoniae* (cKp) and hypervirulent *K. pneumoniae* (hvKp). cKp is more commonly associated with nosocomial infections, immunocompromised patients, and multidrug resistance, whereas hvKp is associated with severe community-acquired invasive infections, including pyogenic liver abscesses, endophthalmitis, meningitis, and metastatic spread of infection, and can affect immunocompetent patients [4]. The virulence of hvKp is not determined by a single marker, but rather by a combination of traits, including overproduction of capsular polysaccharide, a hypermucoviscous phenotype, regulators of capsule synthesis, siderophore systems, lipopolysaccharide, fimbriae, and other determinants of host interaction [4,5]. Among the capsular types frequently associated with hvKp, K1 and K2 occupy a special place, along with K5, K20, K54, and K57 [4,5]. For K2 strains, the association with highly virulent clonal lineages, including ST86, is clinically significant. Thus, in a recent comparative study, ST86 isolates demonstrated the highest virulence indices and were predominantly associated with capsular type K2 [6].

Capsular polysaccharide (CPS) contributes to the pathogenicity of *K. pneumoniae* by protecting cells from phagocytosis, opsonization, and complement-mediated killing [2,7,8]. The diversity of capsular loci complicates antimicrobial approaches directed at the bacterial surface. The capsule also serves as a receptor or substrate for capsule-targeting phages and their depolymerases [8,9].

Bacteriophages and phage-derived enzymes offer approaches to controlling *K. pneumoniae* strains resistant to several classes of antibiotics [10–13]. Their activity depends on bacterial surface structures, including the capsule and O-antigen, and on host defense systems [12]. Characterization of new isolates therefore includes their host activity, replication parameters, effects on biofilms, and genome content [10,12,14,15].

Capsule-specific *K. pneumoniae* phages are of particular interest because many of them encode receptor-binding proteins with polysaccharide depolymerase activity. Such enzymes are usually components of tail fibers or tailspikes, recognize specific surface polysaccharides, and degrade CPS, thereby facilitating phage adsorption and subsequent infection of the cell [9,16,17]. Depolymerases can also be considered independent anti-virulence agents: by promoting removal or partial degradation of the capsule, they increase the susceptibility of *K. pneumoniae* to complement-mediated killing, phagocytosis, and other mechanisms of innate defense [8,16]. At the same time, the activity of these enzymes usually remains capsule-specific; therefore, the search for new depolymerases targeting clinically significant CPS variants represents a separate line of research [9,16,17].

To date, a number of bacteriophages active against *K. pneumoniae* capsular type K2 have been characterized. Solovieva et al. described a group of podoviruses lytic for hypermucoviscous strains of capsular types K1, K2, and K57, including the K2-targeting phages KpV74 and KpV763 [18]. The KpV74-associated depolymerase Dep_kpv74 was subsequently studied and shown to degrade K2 CPS and exert a protective effect in an experimental infection model [19]. Other studies have also expanded the set of K2-specific phages and depolymerases: phages active against K2-expressing hvKp or CRKP strains

have been described, including a phage targeting strain 52145 [20], PSKP16 [21], Kpp-9 [22], vB_KlebPS_265 [23], HHU1 [24], vB_KpnM_JYSS3 encoding the depolymerase Dep17 [16], P12L [25], as well as phage depolymerases directed against K2 CPS [17,26]. These studies demonstrate that K2-targeting phages differ substantially in taxonomy, morphology, host range, replication kinetics, antibiofilm activity, and the repertoire of genes encoding putative receptor-binding proteins.

The genus *Sircambvirus*, within the subfamily *Jameshumphriesvirinae* and class *Caudoviricetes*, includes tailed double-stranded DNA phages of *Klebsiella* [27]. A characterized K2-targeting representative, KpTRp1, was isolated from wastewater in Tunisia and assigned to *Sircambvirus* by genomic analysis [28]. It had a narrow host range, a reported latent period of approximately 30 min, and a burst size of approximately 6 PFU per infected cell; no antibiotic resistance or lysogeny genes were detected. Additional isolates are needed to establish how much biological and genomic diversity occurs among K2-targeting *Sircambvirus* phages and how their capsule-recognition proteins relate to those of other phage lineages.

The diversity of capsule-recognition proteins also raises an evolutionary question: how are similar receptor-binding functions maintained in phages with different genomic backgrounds and virion structures? Botstein's theory of modular phage evolution proposed that phage genomes evolve through the exchange and reassortment of genetic units with distinct functions [29]. Comparisons of whole genomes, individual virion proteins, and separate regions of receptor-binding proteins can reveal how this modular organization is expressed at different levels of phage structure. However, the biological diversity of K2-targeting *Sircambvirus* phages remains incompletely characterized, and the extent to which the evolutionary histories of conserved virion proteins and distinct tailspike regions reflect whole-genome relationships remains insufficiently understood.

The aim of this study was to characterize three newly isolated K2-targeting phages, Kleo, Medik, and Spark, and to investigate their genomic relationships and patterns of modular evolution at the genome and tailspike levels. Using the hypervirulent and hypermucoviscous K2 strain *K. pneumoniae* KPi1627 as the propagation host [18,19], we examined phage morphology, host activity, adsorption-associated titer changes, post-adsorption growth kinetics, antibiofilm activity, and survival outcomes in the *Galleria mellonella* infection model. The additional Spark-susceptible isolate M190 was characterized genomically to establish its bacterial lineage and resistance profile. Comparative genomic analyses were performed to determine the relationships of the three phages within *Sircambvirus* and a broader *Jameshumphriesvirinae*-associated group. Whole-genome and gene-sharing relationships were compared with phylogenies based on the major capsid protein (MCP), the large terminase subunit (TLS), and separate tailspike regions to assess potential evidence of modular evolution.

## 2. Materials and Methods

### *2.1. Bacterial Strains and Culture Conditions*

The clinical isolate *Klebsiella pneumoniae* KPi1627 (Culture collection number SCPM-O-B-7849; GenBank: JADOFI000000000.1), belonging to the O1:K2 serotype, ST86, was obtained from the State Collection of Pathogenic Microorganisms and Cell Cultures (SCPM, Obolensk, Russia) and served as the host strain for phage isolation and propagation. The strain was maintained as a sterile glycerol stock (30% $v/v$) at −80 °C. For routine cultivation, bacteria were grown in LB broth (Lennox; Difco, BD, Franklin Lakes, NJ, USA) at 37 °C with shaking at 250 rpm. Solid media consisted of LB agar plates prepared from the same LB formulation supplemented with 1.5% ($w/v$) agar, while LB soft agar (0.75% $w/v$ agar) was used for the double-layer agar overlay technique.

### *2.2. Isolation of Bacteriophages from Natural Sources, Cultivation, and Storage Conditions*

Three bacteriophages, Kleo, Medik, and Spark, were isolated from surface water samples collected at three sites in the Moscow Region, Russia: the Pakhra River (Kleo), the pond of Klenovskoe settlement (Medik), and the Yuzhny pond in Podolsk, Kutuzovo microdistrict (Spark).

For each sample, 20 mL was first clarified by centrifugation at 8000× *g* for 15 min (Nuve NF 1200 R, NÜVE, Ankara, Turkey) and then filtered through a 0.22-µm membrane filter (Guangzhou Jet Bio-Filtration Co., Ltd., Guangzhou, China). The filtrate was supplemented with 10 mL of 3× LB broth and 200 µL of an overnight culture of *K. pneumoniae* KPi1627. The mixture was incubated overnight at 37 °C with shaking at 210 rpm in an Orbital Shaker Incubator ES-20 (BioSan, Riga, Latvia). After incubation, chloroform (Aldosa, Moscow, Russia) was added to a final concentration of 5% (*v*/*v*), and the mixture was incubated for an additional 15 min at the same temperature before centrifugation at 10,000× *g* for 15 min in a Microspin 12 centrifuge (BioSan, Riga, Latvia). The presence of phages in the supernatant was confirmed using the double-agar overlay method with 0.75% LB soft agar. Ten-fold serial dilutions of the phage-containing supernatant were plated onto a bacterial lawn of *K. pneumoniae* KPi1627. A well-isolated plaque was picked, transferred into 950 µL of SM buffer (50 mM Tris-HCl, 100 mM NaCl, 8 mM $MgSO_4$, pH 7.5), treated with 50 µL of chloroform, and centrifuged as above.

To produce high-titer stocks, 40 mL of an overnight culture of *K. pneumoniae* KPi1627 was pelleted (8000× *g*, 15 min) and resuspended in 10 mL of LB broth supplemented with 100 µL of 1 M $MgCl_2$. The suspension was inoculated with the respective plaque lysate at an MOI of 0.01 and incubated at 37 °C for 30 min without shaking to allow adsorption. The mixture was then transferred into 400 mL of LB broth and incubated overnight at 37 °C with shaking. The resulting lysate was treated with chloroform (5%, 15 min, 37 °C) and clarified by centrifugation. Phage particles were precipitated by adding PEG 8000 to a final concentration of 10% (*w*/*v*) (CDH, Daryaganj, Delhi, India) and NaCl to a final concentration of 0.5 M, followed by centrifugation at 8000× *g*. The pellet was resuspended in SM buffer and subjected to an additional centrifugation step at 13,000× *g* for 90 min. The final pellet was dissolved in SM buffer (50 mM Tris-HCl, 100 mM NaCl, 8 mM $MgSO_4$, pH 7.5) to obtain the purified phage stock, which was stored at 4 °C until further use. All three phages were processed identically.

### *2.3. Transmission Electron Microscopy (TEM)*

For morphological examination by negative-stain TEM, bacteriophages were first purified from high-titer lysates. A 30 mL aliquot of phage stock (~1 × $10^8$ PFU/mL) was clarified by low-speed centrifugation and filtered through a 0.22 µm membrane filter to remove bacterial debris. The filtrate was then subjected to ultracentrifugation at 75,000× *g* for 1.5 h at 4 °C using a Hitachi CP100WX preparative ultracentrifuge (Hitachi Koki Co., Ltd., Hitachinaka, Ibaraki, Japan) equipped with a P50AT2 rotor. The supernatant was discarded, the pellet was gently resuspended in 0.1 M ammonium acetate, and the ultracentrifugation step was repeated twice more (75,000× *g*, 4 °C) for 1 h each. After the third wash, the final pellet was resuspended in 1 mL of SM buffer and stored at 4 °C for no longer than two weeks.

For negative staining, specimens were placed onto grids coated with Formvar film and, after drying, treated with a 0.3% aqueous solution of uranyl acetate at pH 4.0. The specimens were examined using a JEM-1400 Plus transmission electron microscope (JEOL, Tokyo, Japan) operated at an accelerating voltage of 80 kV. Phage dimensions were determined by measuring individual virions on calibrated micrographs.

### *2.4. Determination of Phage Host Range*

The host activity of the phages was tested against 13 *K. pneumoniae* strains representing nine capsular types: 12 strains of types K1, K2, K10, K20, K23, K39, K47, and K57, and the clinical isolate M190, assigned to capsule locus type KL13. Bacterial lawns were prepared using the double-layer agar method [30]. A 200 µL aliquot of each bacterial culture grown to $OD_{600}$ = 0.4 (approximately $1 \times 10^8$ CFU/mL) was mixed with 3 mL of 0.75% LB soft agar and poured onto an LB agar plate. Phage suspensions (approximately $1 \times 10^7$ PFU/mL) were initially screened by spotting 10 µL onto the bacterial lawns in triplicate. The plates were incubated at 37 °C for 18–24 h and examined for lysis zones or plaques [31]. The presence of a clear lysis zone was recorded as a positive spot-test result. For Kleo and Medik on strain M190, no lysis was detected during the initial screening at approximately $1 \times 10^7$ PFU/mL, whereas individual plaques were observed with undiluted high-titer phage suspensions (on the order of $10^{10}$ PFU/mL); these interactions were recorded as +/−. Spark produced a positive spot-test result on M190 at the initial screening titer.

For phage–host combinations exhibiting plaque formation, the efficiency of plating (EOP) was determined using serial tenfold dilutions of the phage suspensions. Aliquots of 10 µL were applied to bacterial lawns, and phage titers (PFU/mL) were calculated from plaque counts obtained at suitable dilutions, taking into account the dilution factor and applied volume. EOP was calculated as the ratio of the arithmetic mean titer on the test strain to the arithmetic mean titer on the reference host KPi1627 across three independent replicates [31]. The same procedure was applied to M190, including Kleo and Medik, for which plaques were detected only at high phage concentrations. With a 10-µL spot volume, a single plaque in an undiluted sample corresponds to a theoretical detection threshold of 100 PFU/mL. The corresponding EOP threshold depends on the reference-host titer and ranged from approximately $1.3 \times 10^{-9}$ to $2.1 \times 10^{-9}$ for Kleo and Medik across the replicates. Given the low plaque counts, the resulting EOP estimates were interpreted cautiously. Individual plaque counts, the corresponding dilutions, and reference-host titers for each replicate on M190 are provided in Supplementary Table S4. All experiments were performed in three independent replicates.

### *2.5. Isolation of Phage and Bacterial DNA*

Phage DNA was isolated using a standard phenol-chloroform extraction protocol with minor modifications [32]. Briefly, 250 µL of a high-titer phage lysate (≥$10^8$ PFU/mL) was mixed with 25 µL of DNase I buffer (10 mM Tris-HCl, 2.5 mM $MgCl_2$, 0.5 mM $CaCl_2$, pH 7.6) and 2.5 µL of DNase I (Diaem, Moscow, Russia). After incubation at 37 °C for 10 min, the volume was adjusted to 350 µL with Milli-Q water. SDS was added to a final concentration of 1% (*w*/*v*) together with 3 µL of proteinase K (20 mg/mL, Vazyme Biotech, Nanjing, China), and the mixture was incubated at 65 °C for 30 min to disrupt the capsids. An equal volume of a phenol:chloroform (1:1) mixture was added; the sample was vortexed and centrifuged at 13,500× *g* for 5 min. The upper aqueous phase was collected, mixed with 400 µL of chloroform, vortexed, and centrifuged again at 13,500× *g* for 5 min. DNA was precipitated by adding 0.6 volumes of isopropanol and 10 µL of 5 M NaCl, followed by incubation at −20 °C for 20 min. After centrifugation for 15 min, the DNA pellet was washed with 70% ethanol, centrifuged for 5 min, air-dried, and dissolved in sterile water.

Total DNA was extracted from a clinical isolate of *K. pneumoniae* using the MagPure Pathogen DNA/RNA Enrich Kit (Magen, Guangzhou, China) according to the manufacturer's instructions. The DNA was then purified from RNA by on-bead RNase A (10 mg/mL, Biolabmix, Novosibirsk, Russia) treatment using the same magnetic particles.

The concentration of the extracted phage and bacterial DNA and the prepared libraries was measured using a Fluo-200 fluorometer (AllSheng, Hangzhou, China) with the Equalbit

1× dsDNA HS Assay Kit (Vazyme, Nanjing, China). The integrity of the extracted DNA was assessed by electrophoresis in 1% (*w*/*v*) agarose gel.

### *2.6. Antimicrobial Susceptibility Testing of the Clinical K. pneumoniae Isolate*

Antimicrobial susceptibility testing of the *K. pneumoniae* clinical isolate was performed using the standardized disk diffusion method of the European Committee on Antimicrobial Susceptibility Testing (EUCAST) [33–35]. Several morphologically similar colonies from an 18–24 h culture grown on LB agar medium were suspended in sterile 0.9% saline, and the suspension was adjusted to a 0.5 McFarland turbidity standard. The inoculum was used to uniformly inoculate the entire surface of Mueller–Hinton agar (Bio-Rad Laboratories, Inc., Hercules, CA, USA) plates.

Commercial 6-mm BD BBL™ Sensi-Disc™ antimicrobial susceptibility test discs (Becton, Dickinson and Company, Franklin Lakes, NJ, USA) containing levofloxacin (5 µg), amoxicillin–clavulanic acid (20/10 µg), meropenem (10 µg), gentamicin (10 µg), imipenem (10 µg), cefepime (30 µg), and trimethoprim–sulfamethoxazole (1.25/23.75 µg) were applied to the inoculated agar within 15 min. The plates were placed in the incubator and incubated in ambient air at 35 °C for 20 h.

Inhibition zone diameters were interpreted using the EUCAST Clinical Breakpoint Tables for *Enterobacterales*, version 16.1 [34]. Results were categorized as susceptible, standard dosing regimen (S); susceptible, increased exposure (I); or resistant (R). Individual inhibition-zone diameters, their mean ± standard deviation (SD; $n = 3$), and the corresponding EUCAST susceptibility categories are provided in Supplementary Table S2.

### *2.7. Biological Parameters of Bacteriophage Infections*

The bacterial host (*Klebsiella pneumoniae* strain KPi1627) was grown in LB broth at 37 °C with shaking (180 rpm) using an Orbital Shaker Incubator ES-20 (BioSan, Riga, Latvia). Centrifugation steps were performed in a Microspin 12 centrifuge (BioSan, Riga, Latvia). Phage titers were determined by the soft-agar overlay method: samples were plated on top agar seeded with the host bacterium, and plaques were counted after 24 h of incubation at 37 °C. All experiments were carried out with freshly prepared bacterial cultures in logarithmic phase ($OD_{600} \approx 0.4$, corresponding to ~$1 \times 10^8$ CFU/mL). To evaluate the effect of the initial multiplicity of infection (MOI) on phage yield, a phage stock ($1 \times 10^9$ PFU/mL) was serially diluted, and 100 µL of each dilution (from $10^9$ to $10^4$ PFU/mL) was mixed with 100 µL of bacterial suspension (~$1 \times 10^8$ CFU/mL) in 200 µL LB broth (final volume, 400 µL), giving final MOI values from 10 to $10^{-4}$. The mixtures were incubated overnight at 37 °C with shaking (180 rpm). After centrifugation (8000× *g*, 15 min), the supernatants were collected and titrated to determine phage yield [24,28].

For one-step growth curves, bacteria were pelleted from 20 mL of culture (8000× *g*, 15 min), resuspended in 500 µL LB broth, and infected with phages at an MOI of 0.01. After 5 min of adsorption at 37 °C with shaking (180 rpm), unadsorbed phages were removed by centrifugation (12,000× *g*, 2 min). The infected pellet was resuspended in 1 mL LB broth, transferred to a 15-mL tube, and adjusted to 10 mL with LB broth. The cultures were incubated at 37 °C with shaking (180 rpm), and 100-µL samples were collected every 10 min for 70 min. Each sample was serially diluted in 0.9% NaCl and spotted onto indicator plates for phage titration.

Experimental time zero ($t_0$) was defined as the sampling point immediately after resuspension and dilution of the bacterial pellet in fresh medium following removal of the initial supernatant. This operational reference point was used to describe post-adsorption growth kinetics and was not assumed to coincide with the onset of infection. The first detectable increase in titer was identified from samples collected at 10-min intervals.

Apparent burst size was estimated as the ratio of the mean titer during the first post-rise plateau to the titer at $t_0$. Samples were titrated without separately quantifying free phages and infected cells; consequently, this ratio was interpreted as a method-dependent estimate rather than an independently validated measurement of progeny production per infected cell. Subsequent increases in titer were excluded from this calculation [36,37].

To measure adsorption kinetics, the culture (20 mL) was supplemented with 10 mM $MgCl_2$ and 1 mM $CaCl_2$ to enhance phage attachment [14,38,39]. Phages were added at MOI = 0.001, and the mixture was incubated at 37 °C with gentle shaking (80 rpm). Immediately after phage addition, 100-µL aliquots were collected at 0.5-min intervals for the first 5 min (0, 0.5, 1, 1.5, ... 5 min) and additionally at 10 min post-infection. Each sample (100 µL) was immediately transferred to a tube containing 850 µL of ice-cold SM buffer and 50 µL of chloroform, and kept on ice [40]. Chloroform treatment was used to inactivate bacterial cells and limit their contribution as infectious centers during subsequent plaque assays. A chloroform-based approach to adsorption measurements has previously been described by Nabergoj et al. [41]. After centrifugation (10,000× *g*, 10 min), the supernatants were titrated to determine the concentration of recoverable infectious phages. The reference titer ($P_0$) was determined from the sample collected at t = 0 and processed identically to all subsequent samples, including dilution in ice-cold SM buffer, chloroform treatment, centrifugation, and titration. At each subsequent sampling time, the recoverable infectious phage titer (P) was expressed relative to this reference as $P/P_0 \times 100\%$. Apparent adsorption was calculated as $(1 - P/P_0) \times 100\%$. Because chloroform treatment may affect the recovery of reversibly attached phages and potentially release mature intracellular progeny at later stages, these measurements were interpreted as operational estimates of adsorption kinetics rather than absolute quantification of irreversible phage attachment [42].

All experiments were performed in three independent biological replicates.

### *2.8. Evaluation of Bacteriophage Activity Against Preformed K. pneumoniae Biofilms*

Biofilms of *Klebsiella pneumoniae* were established in sterile flat-bottom 96-well polystyrene microplates (Nest Biotechnology, Wuxi, China). An overnight bacterial culture was diluted to approximately $10^6$ CFU/mL in PBS. Each well was inoculated with 100 µL of the bacterial suspension and 100 µL of fresh brain heart infusion (BHI) broth. The plates were incubated statically at 37 °C for 24 h to allow biofilm formation.

Following incubation, the planktonic culture was removed, and the established biofilms were gently washed 3 times with 300 µL of sterile PBS. The biofilms were subsequently treated with 100 µL of phage suspension at concentrations of $10^7$, $10^6$, $10^5$, $10^4$, or $10^3$ PFU/mL. These phage doses were designated nominal input MOIs of 10, 1, 0.1, 0.01, and 0.001 based on the initial bacterial inoculum.

After 24 h of phage exposure, the supernatants were removed, and the wells were gently washed three times with 300 µL of sterile PBS to remove planktonic and loosely attached cells. The remaining attached biofilms were fixed with 200 µL of methanol for 30 min. After removal of the methanol, the plates were air-dried. The fixed biofilms were stained with 200 µL of 0.1% (*w*/*v*) crystal violet for 20 min at room temperature. Excess stain was removed by washing the wells three times with PBS, after which the plates were air-dried.

The biofilm-bound crystal violet was solubilized with 250 µL of 33% (*v*/*v*) acetic acid. Absorbance was measured at 595 nm using a microplate spectrophotometer (Hangzhou Miu Instruments Co., Ltd., Hangzhou, China). Blank-corrected absorbance values were calculated by subtracting the mean absorbance of bacteria-free control wells from the corresponding sample values.

The experiment was performed in three independent biological replicates, with 3 technical replicate wells per condition in each experiment. Technical replicate values were

averaged before statistical analysis. Data are presented as the mean ± standard deviation of the independent experiments.

### *2.9. Evaluation of Phage Activity In Vivo Using the Galleria mellonella Model*

*Galleria mellonella* larvae have been introduced as an alternative model to evaluate the efficacy of phage therapy [43]. Larvae of *G. mellonella* were obtained from a local vendor. *G. mellonella* larvae were stored upon arrival in a ventilated glass jar in the dark at room temperature and were used in experiments within 24 h after obtaining.

The *K. pneumoniae* inoculum was prepared from an overnight culture diluted 1:100 and grown to $OD_{600}$ 0.6–0.8. Cells were centrifuged, resuspended in saline to ~$1 \times 10^8$ CFU/mL, serially diluted to ~$1 \times 10^4$ CFU/mL, and used for injection.

Phages used for treatment were purified by PEG precipitation (10% PEG 8000; CDH, Daryaganj, India), resuspended in 0.9% NaCl, and titrated. Phage suspension concentrations for the experiments ranged from $1 \times 10^5$ PFU/mL to $1 \times 10^2$ PFU/mL, in accordance with each MOI.

The therapeutic efficacy of three phages was assessed in a *G. mellonella* larval infection model. Larvae were first infected with bacteria and then treated with a phage injection. In short, 10 µL of a mid-log-phase *K. pneumoniae* suspension was injected into the posterior left proleg of each larva. One hour after bacterial injection, 10 µL of a phage suspension was delivered into the posterior right proleg at nominal input MOIs of 10, 1, 0.1, and 0.01. These ratios were calculated from the administered PFU and the initial bacterial inoculum, rather than the bacterial population present at treatment.

Treated larvae were placed in Petri dishes ($n = 5$ for each dish to avoid competition for food and cannibalism) and incubated at 37 °C and 70% relative humidity in the dark. Larval survival was monitored and recorded every 24 h for 120 h to assess the dose-dependent therapeutic effect. *G. mellonella* larvae were considered deceased when they demonstrated no motor response to touch.

Three control groups were included in each experiment. The bacteria-only control received 10 µL of *K. pneumoniae* suspension followed 1 h later by 10 µL of 0.9% NaCl. The negative control received two 10 µL injections of 0.9% NaCl 1 h apart. The phage-only control received 10 µL of 0.9% NaCl followed 1 h later by 10 µL of phage suspension at $1 \times 10^5$ PFU/mL.

One experimental series was conducted for each phage. Each series comprised four phage-treatment groups and three control groups, with 25 larvae per group (175 larvae per phage).

### *2.10. Statistical Analysis*

Statistical analysis was performed using GraphPad Prism 10.5.0 (GraphPad Software, Boston, MA, USA). Quantitative data were analyzed using one-way analysis of variance (ANOVA) followed by Tukey's HSD multiple-comparisons test. Different lowercase letters on the graphs indicate statistically significant differences among groups based on Tukey-adjusted *p*-values ($p < 0.05$). Error bars represent the standard deviation (SD) of independent biological replicates unless otherwise stated. Larval survival curves were analyzed using the Kaplan–Meier method and compared using the log-rank (Mantel–Cox) test. Global comparisons were performed separately for each phage. Pairwise comparisons were considered exploratory and are reported using unadjusted *p*-values. As a sensitivity analysis, we additionally report the Holm-adjusted *p*-value for the Spark MOI 10 comparison with the corresponding bacteria-only control, accounting for the four dose-specific comparisons.

### *2.11. Genome Sequence Assembly and Annotation*

DNA libraries were prepared using the VIPGen Fast Library Prep Kit V1.1 (Genterra, Moscow, Russia) according to the manufacturer's protocol. The libraries were circularized and sequenced on the DNBSEQ-G400 platform (MGI Tech Co., Ltd., Shenzhen, China) using paired-end sequencing with read lengths of 100 bp (PE100) and 150 bp (PE150).

Reads obtained for phages Kleo, Medik and Spark were assembled using Unicycler 0.5.1 [44]. Coding sequences were identified and initially annotated using Pharokka v1.9.1 with default settings [45]. Functional annotation of the predicted genes was performed using a combination of sequence similarity- and structure-based approaches. HHpred searches were performed against the PDB_mmCIF70_20_Feb, Pfam-A_v38.2, UniProt-SwissProt-viral70_3_Nov_2021, and NCBI_Conserved_Domains (CD) v3.19 databases using default settings (https://toolkit.tuebingen.mpg.de/tools/hhpred, accessed on 15 May 2026) [46]. DALI searches (http://ekhidna2.biocenter.helsinki.fi/dali/, accessed on 16 May 2026) [47] were performed using protein structures predicted with AlphaFold 3 (https://alphafoldserver.com, accessed on 15 May 2026) [48]. Anti-defense systems were searched using AntiDefenseFinder available through the DefenseFinder web server (https://defensefinder.mdmlab.fr/, accessed on 16 May 2026) [49].

The long-read library for M190 genomic DNA was prepared from 500 ng of high-molecular-weight DNA using the Ligation Sequencing Kit XL V14 (SQK-LSK114-XL; Oxford Nanopore Technologies, Oxford, UK), with enrichment of long fragments using Long Fragment Buffer according to the manufacturer's instructions. The library was sequenced on an R10.4.1 flow cell (FLO-PRO114M) using a PromethION device (Oxford Nanopore Technologies, Oxford, UK) with MinKNOW v23.11.2. The *K. pneumoniae* genome was assembled from long reads using Flye v2.9.3 [50]. The assembly was polished using short reads with Pypolca v0.4.0; subsequent polishing with Polypolish 0.6.0 resulted in no sequence changes [51]. Sequence typing and detection of antimicrobial resistance and virulence determinants were performed using Kleborate v3.2.4 [52], including K- and O-locus typing with the Kaptive module [53]. Plasmid replicons were identified with PlasmidFinder 3.0.3 [54].

### *2.12. Bacteriophage Taxonomic Classification*

Taxonomic names and assignments were interpreted according to ICTV Master Species List 41 (MSL41; 2025 taxonomy release) [27]. Assignments proposed from the analyses performed here are distinguished from ICTV-classified taxa.

### *2.13. Comparative Genome Mapping*

Comparative genome maps were generated with clinker through the CAGECAT web server using default settings (https://cagecat.bioinformatics.nl/, accessed on 16 May 2026) [55,56].

### *2.14. Intergenomic Similarity Analysis*

Related phage genomes were identified using BLASTn v2.12.0 searches [57] against the GenBank phage database (GBPHG) (https://www.ncbi.nlm.nih.gov/genbank, accessed on 12 June 2026) with an E-value threshold of 0.05. Intergenomic similarities were calculated using the VIRIDIC web server using default settings (https://rhea.icbm.uni-oldenburg.de/VIRIDIC/, accessed on 12 June 2026) [58].

### *2.15. Proteomic and Phylogenomic Analyses of Phages Kleo, Medik, and Spark*

Proteomic and phylogenomic analyses were performed using ViPTree (https://www.genome.jp/viptree/, accessed on 14 June 2026) [59] and VICTOR (https://ggdc.dsmz.de/victor.php, accessed on 14 June 2026) [60], respectively. For the ViPTree analysis, the

genomes of phages Kleo, Medik, and Spark were uploaded as FASTA files, while reference genomes selected from the BLASTn search results against GBPHG were specified using their NCBI accession numbers. The VICTOR analysis was performed at the nucleotide level using the D0 formula.

### *2.16. MCP- and TLS-Based Phylogenetic Analyses of Phages Kleo, Medik, and Spark*

Candidate homologs were identified using tBLASTn searches against GBPHG, with an E-value threshold of $1 \times 10^{-5}$. MCP candidates were selected based on matches to the MCPs of phages Kleo, Medik, and Spark. TLS candidates were selected based on matches to the ATPase domains of the large terminase subunits of phages Kleo, Medik, and Spark. Amino acid sequences were aligned using MAFFT [61] with the L-INS-i algorithm. The TLS alignment was trimmed manually, taking into account the position of the ATPase domain in the AlphaFold 3-predicted structure of the phage Spark TLS (https://alphafoldserver.com, accessed on 15 May 2026) [48]. Phylogenetic trees based on the MCP and TLS alignments were constructed using IQ-TREE 3.1.2 [62]. The best-fit amino acid substitution model was selected automatically using ModelFinder Plus according to the Bayesian information criterion. Branch support was assessed using 1000 ultrafast bootstrap replicates. All trees were visualized using iTOL v7 (https://itol.embl.de/, accessed on 16 June 2026) [63].

### *2.17. Virulence Factor Screening*

The genomes of phages Kleo, Medik, and Spark were screened for known virulence factor genes using BLASTn and BLASTp searches against the nucleotide and protein sequence datasets, respectively, of the VFDB core dataset (Set A) downloaded from the VFDB website (https://www.mgc.ac.cn/VFs/download.htm, accessed on 28 June 2026) [64]. Searches were performed using an E-value cutoff of 0.05.

### *2.18. Caudoviricetes Genome Dataset*

*Caudoviricetes* genomes were retrieved from the GenBank phage database (GBPHG) (https://www.ncbi.nlm.nih.gov/genbank, accessed on 12 June 2026). All records labelled as UNVERIFIED were manually removed, and only sequences designated as complete genomes were included in the dataset. We selected only genomes classified as members of the class *Caudoviricetes*. Taxonomic classification was performed using geNomad 1.12.0 [65]. Genome completeness was assessed using ViralQC (Git revision fdb9ddc, 16 May 2026) [66]. Sequences with completeness values below 95% and/or confidence values other than high were excluded. This filtering resulted in a final dataset of 20,659 genomes.

### *2.19. Klebsiella Phage Genome Dataset*

*Klebsiella* phage genomes were selected from the *Caudoviricetes* dataset based on the host and lab_host fields. Only genomes for which *Klebsiella pneumoniae*, irrespective of strain, was specified as a host were retained. Phages reported to infect multiple hosts were also included when *Klebsiella pneumoniae* was among the listed hosts. The final dataset comprised 968 genomes.

### *2.20. Genome Dataset Assembly for ViPTree Analysis of Jameshumphriesvirinae*

To assemble the genome dataset for the initial ViPTree analysis, the complete genomes of all ICTV-classified members of the subfamily *Jameshumphriesvirinae* were used as BLAST queries against the *Caudoviricetes* genome dataset described above. The results of all searches were combined, duplicate genomes were removed, and all unique matching genomes were included in the dataset.

The MCPs of all ICTV-classified members of *Jameshumphriesvirinae* were then extracted from their genomes and used as tBLASTn queries against the *Caudoviricetes* genome dataset. For each query, genomes were included up to the first pronounced decrease in bit score, defined as a decrease of at least twofold between consecutive matches. The results from all searches were combined, and duplicate genomes were removed.

TLS-based selection followed the same procedure. However, no pronounced decrease in bit score was observed in the TLS searches. Therefore, all matches were initially retained. When multiple matches corresponded to the same genome, only the match with the highest bit score was kept, and the first 300 genomes ranked by bit score were added to the dataset.

### *2.21. ViPTree Proteomic Analysis of Jameshumphriesvirinae*

Proteomic trees were constructed using ViPTree (https://www.genome.jp/viptree/, accessed on 20 July 2026) [59]. The initial proteomic tree was generated in the ViPTree "With references" mode using the ViPTree reference set together with the assembled genome dataset. This tree was inspected to identify the group containing members of *Jameshumphriesvirinae* and the sister groups positioned close to it. A second tree was subsequently generated in the "Only query" mode using a manually selected dataset of 114 genomes. This dataset included phages that clustered with ICTV-classified members of the subfamily *Jameshumphriesvirinae*, all phages positioned close to the clade of interest, and several representatives of each ICTV-classified sister family or subfamily. Genomes originating from the ViPTree reference set were manually included among the query sequences when relevant.

### *2.22. Identification of MCP and TLS Homologs for Phylogenetic Analysis of Jameshumphriesvirinae*

Candidate homologs were identified using tBLASTn searches against the *Caudoviricetes* genome dataset described above, with an E-value threshold of $1 \times 10^{-5}$. All other tBLASTn parameters were left at their default settings. MCP candidates were selected based on matches to the MCPs of all ICTV-classified phages of the subfamily *Jameshumphriesvirinae*. The final MCP dataset used for tree construction comprised 140 proteins. TLS candidates were selected based on matches to the ATPase domains of the large terminase subunits of all ICTV-classified phages of the subfamily *Jameshumphriesvirinae*. The final TLS dataset used for tree construction comprised 332 proteins.

### *2.23. Multiple Sequence Alignment and Phylogenetic Analysis of Jameshumphriesvirinae*

The full-length amino acid sequences were aligned using MAFFT [61] with the L-INS-i algorithm. The TLS alignment was then trimmed manually to retain the ATPase domain, taking into account the domain boundaries corresponding to residues 1–288 of the full-length phage Spark TLS in its AlphaFold 3-predicted structure.

Phylogenetic trees based on the MCP alignment and the trimmed TLS ATPase-domain alignment were constructed using IQ-TREE 3.1.2 [62]. The best-fit amino acid substitution model was selected automatically using ModelFinder Plus according to the Bayesian information criterion. Branch support was assessed using 1000 ultrafast bootstrap replicates. All trees were visualized using iTOL v7 (https://itol.embl.de/, accessed on 20 July 2026) [63].

### *2.24. Analysis of Capsule-Specific Receptor-Binding Proteins*

Putative capsule-specific receptor-binding proteins (tailspike proteins, TSPs) in phages Kleo, Medik, and Spark were identified using tBLASTn searches with Dep_kpv79 from *Klebsiella* phage vB_KpnM_KpV79 as the query. Protein structures were predicted using AlphaFold 3. Structural visualization and superposition were performed using UCSF

ChimeraX 1.12. Structural searches against DepoCat, a catalog of experimentally characterized *Klebsiella* phage depolymerases, were performed using US-align [67,68].

To compare TSP conservation with that of other genes, all annotated proteins in the three genomes were compared using local alignments in Biopython 1.85 with the BLOSUM62 substitution matrix, a gap-opening score of −10, and a gap-extension score of −0.5 [69]. Candidate homologs were required to be at least 50 amino acids long and to share at least 30% identity, with aligned residue pairs covering at least 80% of each protein. Groups were retained when all three pairwise comparisons were reciprocal unique best-scoring matches; groups containing a protein with a within-genome paralog meeting the same criteria were excluded. Each retained protein pair was aligned globally with the same scoring scheme, and the alignment was back-translated to the corresponding CDSs.

Two separate datasets were generated for phylogenetic analysis of the N-terminal and depolymerase regions. Candidates for both datasets were selected using tBLASTn searches against the *Caudoviricetes* genome dataset described above, with the corresponding N-terminal or depolymerase region of the phage Spark TSP used as the query and an E-value threshold of 0.05. All other tBLASTn parameters were left at their default settings. The TSP of *Shigella* phage Sf6 was additionally included in the depolymerase-region dataset based on its structural similarity to the phage Spark TSP identified by a DALI search against the PDB (http://ekhidna2.biocenter.helsinki.fi/dali/, accessed on 5 August 2026).

Amino acid sequences in both datasets were aligned using MAFFT with the L-INS-i algorithm. The N-terminal- and depolymerase-region alignments were then trimmed manually according to the corresponding regions of the phage Spark TSP. Residues 1–81 were defined as the N-terminal region, whereas residues 82–668 were defined as the depolymerase-containing region, including the downstream C-terminal portion, for the purposes of this analysis. Phylogenetic trees based on the trimmed N-terminal- and depolymerase-region alignments were constructed using IQ-TREE 3.1.2. The best-fit amino acid substitution model was selected automatically using ModelFinder Plus according to the Bayesian information criterion. Branch support was assessed using 1000 ultrafast bootstrap replicates.

### *2.25. Whole-Genome and Gene-Sharing Network Analyses*

For network analysis, a combined phage genome dataset was assembled from the genome sets represented in the MCP, TLS, TSP N-terminal-region, TSP depolymerase-region, and ViPTree analyses. Repeated records were removed, yielding 452 genome records. The accession numbers and descriptions of all 452 genome records are provided in Supplementary Table S3.

Coding sequences were predicted and initially annotated using Pharokka v1.9.1 [45]. Whole-genome nucleotide similarity was calculated with Vclust v1.3.1 [70]. The align command was run in an all-versus-all mode without preliminary k-mer filtering. For 452 genomes, 101,926 unordered genome pairs were compared. Results were saved in complete output format (–outfmt complete). Genome clustering was performed with the cluster command using complete linkage (–algorithm complete) and tANI as the similarity metric. Operational species- and genus-level clusters were defined at tANI thresholds of 0.95 and 0.70, respectively.

Gene-sharing analysis was performed with vConTACT3 v3.2.4 [71] in protein mode using the v232 reference database, the bacterial domain, and the SqRoot intergenomic distance metric. Taxonomic assignments were obtained from the full network containing reference genomes. An induced subgraph containing only genomes from the 452-genome dataset was then extracted for subsequent analysis and visualization. Networks were visualized in Cytoscape v3.10.4 [72].

For quantitative analysis of gene-sharing relationships, the complete user-only vConTACT3 graph at identity layer 0.3 was used; this graph contained 36,049 edges. For Vclust visualization, all pairwise relationships with tANI ≥ 0.70 were retained, with species-level relationships defined at tANI ≥ 0.95. Because visualization of all vConTACT3 edges produced a densely connected graph, a sparsified copy was generated solely for visualization of the network results. For each connected component, a maximum spanning tree was retained using the number of shared protein clusters (shared_genes) as the edge weight. In addition, for each node, up to three incident edges with the highest shared_genes values were retained, together with all edges with shared_genes ≥ 90. The reduced graph was used only for visualization; quantitative edge-count analyses were performed using the complete graph. In the vConTACT3 panels, edge width represented shared_genes, whereas edge opacity represented 1 − SqRoot distance. Node positions were kept consistent between comparative panels.

### *2.26. Synteny and Recombination Analyses*

Whole-genome nucleotide alignments were generated using progressiveMauve (version snapshot_2015_02_13) [73] and retained in XMFA format. Quantitative synteny was assessed using these alignments and CDS annotations obtained from Pharokka. Only alignment columns containing unambiguous A/C/G/T nucleotides in both genomes were considered. Nucleotide alignment segments were retained as anchors when they contained at least 250 eligible positions with at least 70% identity. Genome pairs were included when at least 70% of each genome was covered by eligible alignment columns and at least 50% by the selected nucleotide anchors. Corresponding CDSs were identified as reciprocal unique best matches based on the number of jointly aligned nucleotides, requiring at least 60 eligible positions, 70% nucleotide identity, and 70% coverage of each CDS. Gene order and relative orientation were compared after accounting for differences in sequence origin. Immediate gene adjacency was considered conserved only when matched CDSs were directly adjacent among all annotated CDSs in both genomes. The fraction of conserved immediate adjacencies was calculated relative to the number of potential adjacencies between matched CDSs $(n - 1)$. Candidate inversions were evaluated based on reverse-orientation matches and the presence of concordant flanking regions.

For GARD analysis, the 54 selected tail-associated amino acid sequences were reduced independently with CD-HIT v4.8.1 [74] at 99%, 98%, and 97% identity, requiring at least 90% coverage of both sequences; the resulting sets contained 37, 29, and 24 representatives, respectively. Each set was clustered separately using MMseqs2 v18.8cc5c (easy-cluster; coverage ≥ 80%; E-value ≤ 0.001) [75]. Five TSP datasets were selected: the vB_KleM_KB2 group (six sequences; 97% threshold); the same group supplemented with Kleo, Spark, and Medik (nine sequences); the RCIP0080 group (five sequences; 97%); the Ptero group (12 sequences; 98%); and an expanded Ptero selection (18 sequences; 99%). The group names refer to representative phages and do not denote taxonomic units.

Each group was aligned independently with MAFFT v7.526 using L-INS-i (–localpair –maxiterate 1000). GARD in HyPhy [76] was run with the LG amino acid substitution model and general discrete rate variation with four categories. A genetic algorithm searched for breakpoint configurations, and models were selected by the minimum small-sample corrected Akaike information criterion (AICc). Topological incongruence was assessed by comparing the selected model with a model retaining the same partitions and independently estimated branch lengths but a common topology. Breakpoints are reported after the indicated 1-based amino acid alignment columns, including gaps; independently aligned groups have separate coordinate systems. Pairwise identity and residue differences were

calculated within the selected segments of the vB_KleM_KB2 group. Aligned inputs, GARD outputs, segment trees, and numerical summaries are provided in Supplementary File S1.

MCP-oriented comparative genome maps were generated using the Python library Matplotlib (v3.10.8), based on annotated CDS coordinates from Pharokka and pairwise local nucleotide similarities identified by BLASTn. Genome sequences were computationally reoriented relative to the major capsid protein (MCP) to facilitate comparison. CDSs were colored according to their annotated functions, and connecting ribbons represented locally aligned nucleotide regions, with shading indicating sequence identity (Supplementary Figures S6 and S7).

Three TSP search datasets were assembled using separate tBLASTn searches against the GenBank phage database (GBPHG), with the TSP amino acid sequences of Kleo, Spark, and Medik as queries. Genome accessions and hit coordinates were retained. *Kagunavirus* records, vB_KpnM_cmc20193 (MT559528.1), DP01 (PP824815.1), and KlebP_265 (PQ480913.1) were excluded from these search datasets, as was the standalone Dep17 gene record (PQ843046.1). The retained local matches had at least 70% amino acid identity to the corresponding query. Full annotated CDSs containing the hits were extracted in the coding orientation, yielding datasets of 23, 25, and 25 sequences. A separate dataset retained all 54 selected tail-associated CDSs from the *Jameshumphriesvirinae*-associated group, including candidates lacking a specific TSP annotation. The three searches recovered the same 22 retained reference-phage homologues. The Kleo-query dataset contained Kleo and these 22 references, whereas the identical Spark- and Medik-query datasets additionally contained Spark and Medik. A single comparative map is therefore presented for the shared reference-phage set (Supplementary Figure S7).

Proteins were aligned with MAFFT L-INS-i [61], and the alignments were back-translated using the original codons; terminal stop codons were omitted from the nucleotide alignments. Recombination was analyzed with RDP5CL 5.84 [77]. Initial screening used RDP, GENECONV, MaxChi, Chimaera, and 3Seq; Bootscan and SiScan results were also considered. Candidate intervals and sequence relationships were compared across methods and datasets, with alignment, CDS, and genomic coordinates distinguished. RDP5 input alignments and output files are provided in Supplementary File S1.

## 3. Results

### *3.1. Phage Isolation and Morphological Characterization*

Transmission electron microscopy revealed that phages Kleo, Medik, and Spark exhibited a myovirus morphology, with no apparent morphological differences among them (Figure 1a–f). The virions possessed isometric heads measuring approximately 54 nm from vertex to vertex, connected to contractile tails by narrow necks. In the extended state, the tail sheaths measured approximately 75 nm in length and 13.5 nm in width and exhibited transverse striations. In the contracted state, the sheaths measured approximately 36 nm in length and 16–22 nm in width. A distinct baseplate region with peripheral appendages was visible at the distal ends. This morphology is consistent with that previously reported for the K2-targeting *Sircambvirus* phage KpTRp1 [28].

Phages Kleo, Medik, and Spark formed well-defined plaques on a double-layer LB agar lawn of *K. pneumoniae* KPi1627 (Figure 1g–i). Kleo formed plaques of approximately 8 mm in total diameter, with a central lysis zone of approximately 2 mm. Medik produced plaques with a total diameter of approximately 8 mm, including a central lysis zone of approximately 3.5 mm in diameter. Spark produced the largest plaques, with a total diameter of approximately 12 mm and a central lysis zone of approximately 5 mm. Such halo formation is commonly associated with the diffusion of phage-encoded polysaccharide depolymerases and degradation of the bacterial capsule [78,79].

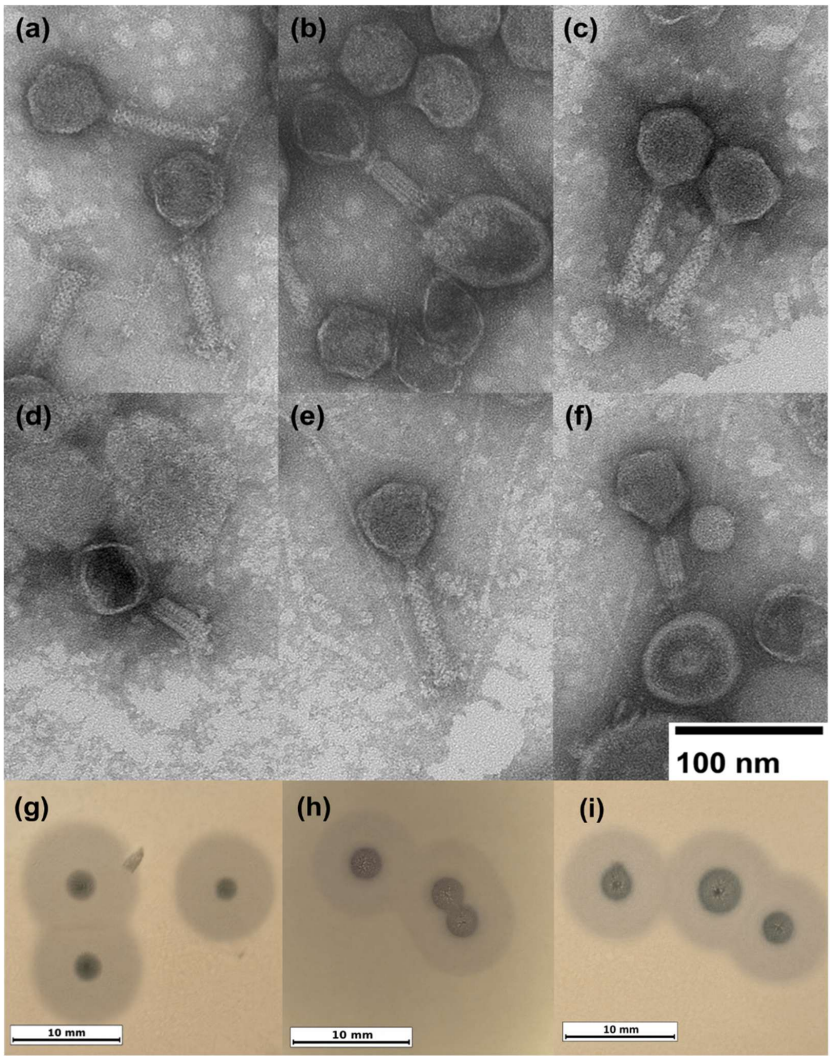



**Figure 1.** Representative transmission electron micrographs and plaque morphology of *Sircambvirus* phages Kleo, Medik, and Spark. Virions of (**a**,**b**) phage Kleo, (**c**,**d**) phage Medik, and (**e**,**f**) phage Spark are shown; scale bar: 100 nm. Plaque morphology of (**g**) phage Kleo, (**h**) phage Medik, and (**i**) phage Spark on a double-layer LB agar lawn of the host strain *Klebsiella pneumoniae* KPi1627; scale bars: 10 mm.

### *3.2. Host Range of Bacteriophages Kleo, Medik, and Spark Against K. pneumoniae Capsular Types*

The host activity of Kleo, Medik, and Spark was evaluated against 13 *K. pneumoniae* strains representing nine capsular types (Table 1). All three were active against the two K2 strains, KPi1627 and KPB4010. This restricted pattern is consistent with that reported for the K2-targeting *Sircambvirus* phage KpTRp1 [28]. Spark exhibited substantially higher plating efficiency on the KL13 isolate M190 (EOP = $1.75 \times 10^{-3}$), with countable plaques obtained at a $10^{-5}$ dilution. In contrast, Kleo and Medik produced 10–15 and 11–18 plaques, respectively, per 10-µL spot of undiluted phage suspensions, corresponding to EOP values of $1.76 \times 10^{-8}$ and $2.78 \times 10^{-8}$. Although these plaque counts exceeded the theoretical single-plaque detection threshold, the extremely low EOP values indicate low-frequency plaque formation and do not establish efficient phage propagation on M190. The corresponding replicate-level plaque counts and reference-host titers are provided in Supplementary Table S4. Among non-reference strains showing plaque formation, EOP values ranged from $1.76 \times 10^{-8}$ to $4.95 \times 10^{-2}$ (Table 1).

**Table 1.** Host activity of phages Kleo, Medik, and Spark against *K. pneumoniae* strains representing different capsular types.

| Designation of *K. pneumoniae* Strain | Culture Collection Number | CPS-Type * | MLST | Carbapenem-Resistance ** | Kleo | | Medik | | Spark | |
|---|---|---|---|---|---|---|---|---|---|---|
| | | | | | Lysis *** | EOP **** | Lysis | EOP | Lysis | EOP |
| M190 | Not available | K13 | ST200 | ACG | +/− | $1.76 \times 10^{-8}$ | +/− | $2.78 \times 10^{-8}$ | + | $1.75 \times 10^{-3}$ |
| KPi1627 | SCPM-O-B-7849 | K2 | ST86 | ACG | + | 1 | + | 1 | + | 1 |
| KPB4010 | SCPM-O-B-7846 | K2 | ST2280 | ACG | + | $2.94 \times 10^{-2}$ | + | $1.04 \times 10^{-2}$ | + | $4.95 \times 10^{-2}$ |
| KPB2580 | SCPM-O-B-7852 | K1 | ST23 | PCG | − | − | − | − | − | − |
| KPi261 | SCPM-O-B-7850 | K1 | ST23 | ACG | − | − | − | − | − | − |
| KPB944 | SCPM-O-B-7882 | K10 | ST147 | PCG | − | − | − | − | − | − |
| KPM9 | SCPM-O-B-7749 | K20 | ST1544 | ACG | − | − | − | − | − | − |
| KPB2304-15 | SCPM-O-B-8047 | K23 | ST11 | S | − | − | − | − | − | − |
| KPB1434-16 | SCPM-O-B-8048 | K39 | ND | ND | − | − | − | − | − | − |
| KPB1224 | SCPM-O-B-7881 | K47 | ST395 | PCG | − | − | − | − | − | − |
| KPB1667 | SCPM-O-B-8043 | K47 | ST395 | PCG | − | − | − | − | − | − |
| KPB542-15 | SCPM-O-B-8042 | K57 | ST23 | ACG | − | − | − | − | − | − |
| KPi8289 | Not available | K57 | ST218 | ACG | − | − | − | − | − | − |

* Capsular type K13 for M190 was inferred from the KL13 locus. ** Carbapenem-resistance information for the previously characterized strains follows [80]; M190 was characterized in this study. ACG, absence of carbapenemase genes; PCG, presence of carbapenemase genes; S, susceptible to meropenem; ND, not determined. *** Symbols: +, lysis was detected in the spot test; −, no lysis was detected in the spot test; +/−, no lysis was detected at the initial phage titer of approximately $1 \times 10^7$ PFU/mL, whereas individual plaques were observed with undiluted high-titer phage suspensions (on the order of $1 \times 10^{10}$ PFU/mL). **** EOP: efficiency of plating relative to the reference host KPi1627, calculated as the ratio of arithmetic mean titers from three independent replicates. Replicate-level data for M190 are provided in Supplementary Table S4. Extremely low EOP values indicate low-frequency plaque formation and do not establish efficient phage propagation.

### *3.3. Genomic and Antimicrobial Characteristics of the K13 Klebsiella pneumoniae Isolate M190*

Long-read assembly followed by short-read polishing yielded a circular chromosome of 5,148,398 bp and a 231,705-bp plasmid for *Klebsiella pneumoniae* M190 (NCBI accession number JCBHEB000000000). In silico MLST assigned the isolate to ST200 within phylogroup Kp1 (*K. pneumoniae* sensu stricto). Surface-polysaccharide genotyping identified capsule locus KL13, associated with capsular type K13, and predicted O-antigen type O3γ. No *ybt*, *clb*, *iuc*, *iro*, or *rmp* loci were detected, and Kleborate assigned M190 a virulence score of 0.

Genomic analysis revealed multiple antimicrobial resistance determinants, including the ESBL gene *blaCTX-M-15*. The genome contained four plasmid-borne copies and one chromosomal copy of *blaCTX-M-15*. No acquired carbapenemase or colistin-resistance genes were detected, and Kleborate assigned the isolate a resistance score of 1. A detailed list of detected resistance determinants is provided in Supplementary Table S1.

Phenotypically, M190 was resistant to amoxicillin–clavulanic acid, cefepime, and trimethoprim–sulfamethoxazole, remained susceptible to gentamicin, imipenem, and meropenem, and was categorized as susceptible at increased exposure (I) to levofloxacin. According to the definition of Magiorakos et al. [81], the isolate met the criteria for multidrug resistance within the antimicrobial panel tested.

### *3.4. Effect of Initial MOI on Phage Yield, Adsorption-Associated Titer Changes, and Post-Adsorption Growth Kinetics*

One-way ANOVA revealed a significant effect of the initial MOI on the final yield of all three phages, Kleo, Medik, and Spark ($p < 0.0001$). Subsequent Tukey's HSD multiple-comparisons tests showed that the highest final titers for each phage were obtained at an MOI of 0.0001, which was the lowest MOI tested (Figure 2a–c). Thus, MOI = 0.0001 provided the highest phage yield within the investigated range, although lower MOIs were not evaluated. This finding is consistent with the reported optimal MOI of 0.0001 for KpTRp1, a K2-specific phage also assigned to the genus *Sircambvirus* [28].

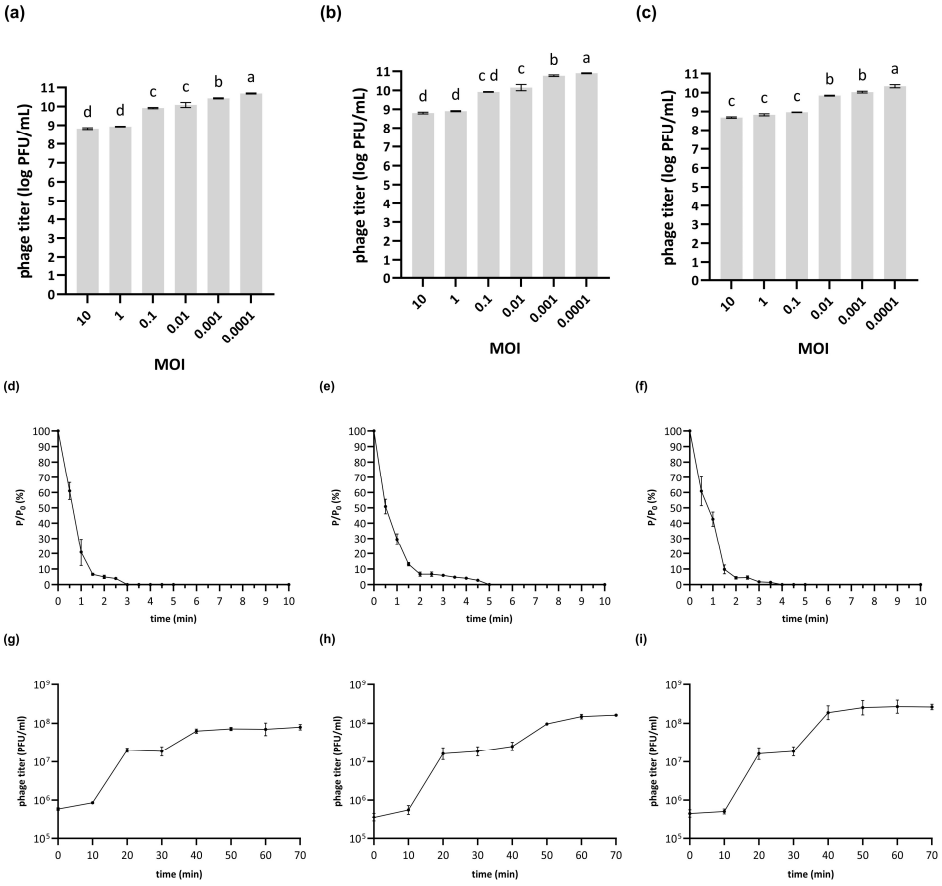



**Figure 2.** Propagation characteristics and infection kinetics of phages Kleo, Medik, and Spark on *Klebsiella pneumoniae* KPi1627. (**a**–**c**) Effect of the initial multiplicity of infection (MOI) on phage propagation. Final titers were determined after overnight propagation of (**a**) Kleo, (**b**) Medik, and (**c**) Spark at the indicated initial MOIs. Different lowercase letters above the columns indicate statistically significant differences among groups according to Tukey's HSD multiple-comparisons test following one-way ANOVA (adjusted $p < 0.05$); the overall effect of MOI was significant for each phage ($p < 0.0001$). (**d**–**f**) Adsorption-associated changes in recoverable infectious phage titers of (**d**) Kleo, (**e**) Medik, and (**f**) Spark at an MOI of 0.001, expressed as the percentage of the initial infectious titer remaining in the chloroform-treated supernatant. These measurements provide operational estimates of adsorption-associated decreases in infectious titers rather than direct measurements of irreversible phage attachment. (**g**–**i**) Post-adsorption growth curves of (**g**) Kleo, (**h**) Medik, and (**i**) Spark at an MOI of 0.01. Experimental time zero ($t_0$) was defined immediately after resuspension and dilution of the bacterial pellet following removal of the initial supernatant and does not denote the onset of infection. Samples were titrated without separate quantification of free-phage and infected-cell fractions. Subsequent increases in titer are presented as observations without assignment to a specific infection mechanism. All values represent the mean ± standard deviation (SD) of three independent biological replicates; error bars indicate SD.

All three phages exhibited a rapid decrease in recoverable infectious titers following exposure to *K. pneumoniae* KPi1627 (Figure 2d–f). After 1 min of incubation, the apparent adsorption values, calculated as $(1 - P/P_0) \times 100\%$, were 79.10% for Kleo, 70.55% for Medik, and 57.36% for Spark. The recoverable infectious phage fraction reached very low levels within approximately 3 min for Kleo, 5 min for Medik, and 4 min for Spark. No recoverable infectious phages were detected in the chloroform-treated supernatants at 3 min for Kleo and 4 min for Spark, whereas the recoverable fraction for Medik reached very low levels by approximately 5 min. Rapid adsorption has also been reported for other *K. pneumoniae* phages, with reported values of 79–93% within 5 min [15]. However, direct quantitative comparison with our apparent adsorption estimates is limited by potential differences in assay procedures. Because the measurements were obtained using a chloroform-based assay, the calculated values should be interpreted as operational estimates rather than direct measurements of irreversible attachment.

The growth curves showed an initial increase in the measured titer between the 10- and 20-min sampling points after the operationally defined post-adsorption $t_0$ (Figure 2g–i). A subsequent increase was observed between 30 and 40 min for Kleo and Spark, and between 40 and 60 min for Medik. These later increases may reflect secondary infection events or differences in the timing of phage release; however, the present experiments do not allow these possibilities to be distinguished. Apparent burst sizes were estimated from the first post-rise plateau relative to the titer at $t_0$, excluding subsequent increases. These values represent operational titer ratios under the assay conditions. The ratios of the mean titers at the first post-rise plateau to the titers at $t_0$ were 27.5 ± 3.7, 45.3 ± 4.5, and 37.3 ± 6.3 for Kleo, Medik, and Spark, respectively.

### *3.5. Bacteriophage-Mediated Reduction in Preformed Klebsiella pneumoniae Biofilm Biomass*

The ability of bacteriophages Kleo, Medik, and Spark to reduce the biomass of 24-h preformed *K. pneumoniae* biofilms was evaluated after a further 24 h of phage exposure. The effects varied according to both the phage and the applied phage concentration, and no monotonic MOI-dependent response was observed (Figure 3a–c).

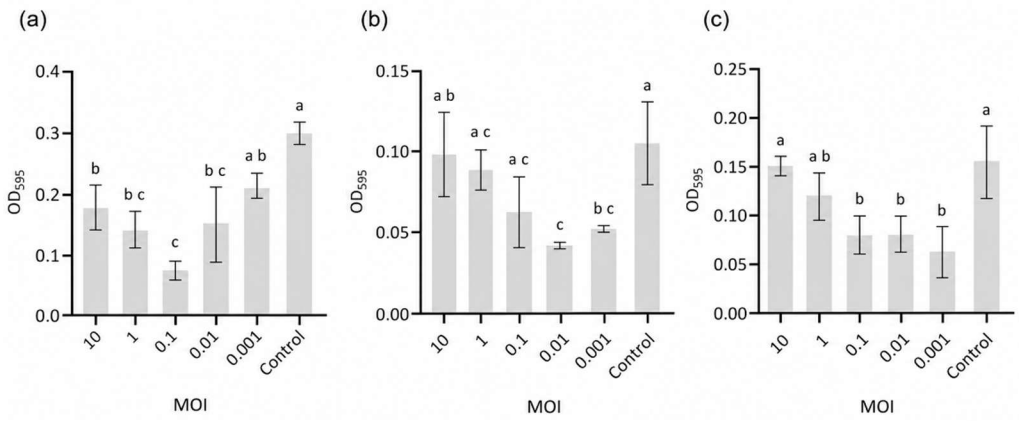



**Figure 3.** (**a**) Concentration dependence of biofilm disruption by phage Kleo. (**b**) Concentration dependence of biofilm disruption by phage Medik. (**c**) Concentration dependence of biofilm disruption by phage Spark. Values are presented as the mean ± SD of three independent biological replicates; error bars indicate SD. Different lowercase letters above the columns indicate significant differences among groups according to Tukey's HSD post hoc test following one-way ANOVA ($p < 0.05$).

For phage Kleo, the greatest reduction in biofilm biomass was observed at a nominal MOI of 0.1 and reached 75.8% relative to the untreated control. For phage Medik, the greatest reduction was observed at a nominal MOI of 0.01 and reached 61.9%. Phage

Spark showed its strongest effect at a nominal MOI of 0.001, reducing biofilm biomass by 59.6%. For all three phages, the greatest reductions in crystal violet-stainable biofilm biomass were observed at relatively low nominal MOIs rather than at the highest phage concentrations tested.

### *3.6. Phage Activity In Vivo in the Galleria mellonella Infection Model*

The therapeutic activity of phages Kleo, Medik, and Spark was evaluated in a *Galleria mellonella* infection model following infection with *K. pneumoniae* KPi1627 and subsequent phage administration at different MOIs (Figure 4a,b).

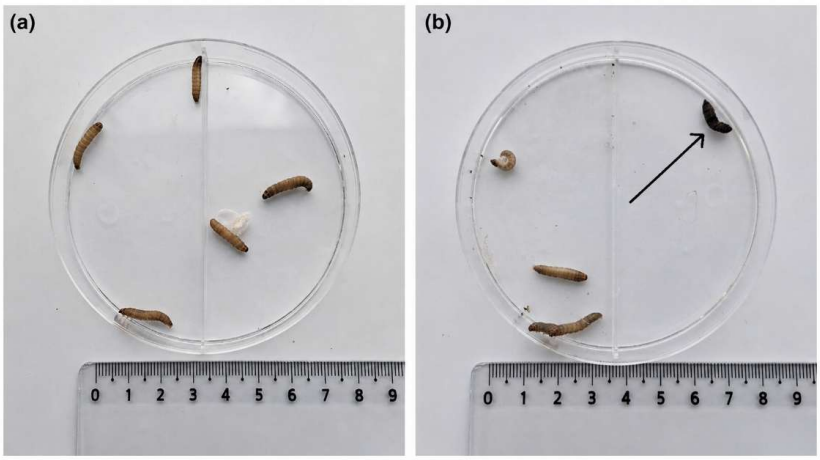



**Figure 4.** *Galleria mellonella* infection model used to evaluate the activity of phages Kleo, Medik, and Spark. (**a**) Larvae before injection. (**b**) Larvae 24 h after injection with *Klebsiella pneumoniae* KPi1627; the dead larva is indicated by an arrow.

Survival outcomes differed among the three phages and depended on the administered MOI (Figure 5a–c). In all three experiments, survival in the bacteria-only control was lower than in the corresponding saline control.

The effect of phage treatment on *Galleria mellonella* survival was evaluated at four multiplicities of infection (MOI 10, 1, 0.1, and 0.01) using the log-rank (Mantel–Cox) test. Pairwise comparisons were considered exploratory and are reported using unadjusted *p*-values. The Holm-adjusted *p*-value is additionally reported for the Spark MOI 10 versus K+ comparison, with adjustment accounting for the four dose-specific comparisons.

In the Kleo experiment, none of the tested MOIs significantly changed larval survival compared with the infected control (K+). The lowest *p*-value was observed at MOI 0.01 ($p = 0.116$), where 10 of 25 larvae (40%) survived to 120 h compared with 5 of 25 (20%) in K+. The global comparison of the five infected groups was also not significant ($\chi^2 = 4.03$, df = 4, $p = 0.402$).

In the Medik experiment, the largest numerical increase in survival was observed at MOI 0.1: 14 of 25 larvae (56%) survived to 120 h compared with 8 of 25 (32%) in K+. However, this difference was not statistically significant ($p = 0.077$). The global log-rank test also did not reach the conventional significance threshold ($\chi^2 = 9.36$, df = 4, $p = 0.0527$).

In the Spark experiment, treatment at MOI 10 was associated with a numerical increase in survival. At 120 h, 15 of 25 larvae (60%) were alive in the MOI 10 group compared with 7 of 25 (28%) in K+. The pairwise log-rank test yielded a nominally significant result ($\chi^2 = 5.19$, df = 1, unadjusted $p = 0.0228$). However, this difference did not remain statistically significant after Holm correction for the four dose-specific comparisons with K+ (adjusted $p = 0.0912$). Survival at MOI 1 was 48% ($p = 0.175$), whereas MOI 0.1 and MOI 0.01 resulted in final survival of 28% ($p = 0.633$) and 12% ($p = 0.137$), respectively. The

global comparison of the five survival curves was significant ($\chi^2 = 16.02$, df = 4, $p = 0.0030$). In contrast, pooling all MOI groups into a single treatment group did not reveal an overall difference from K+ ($p = 0.541$).

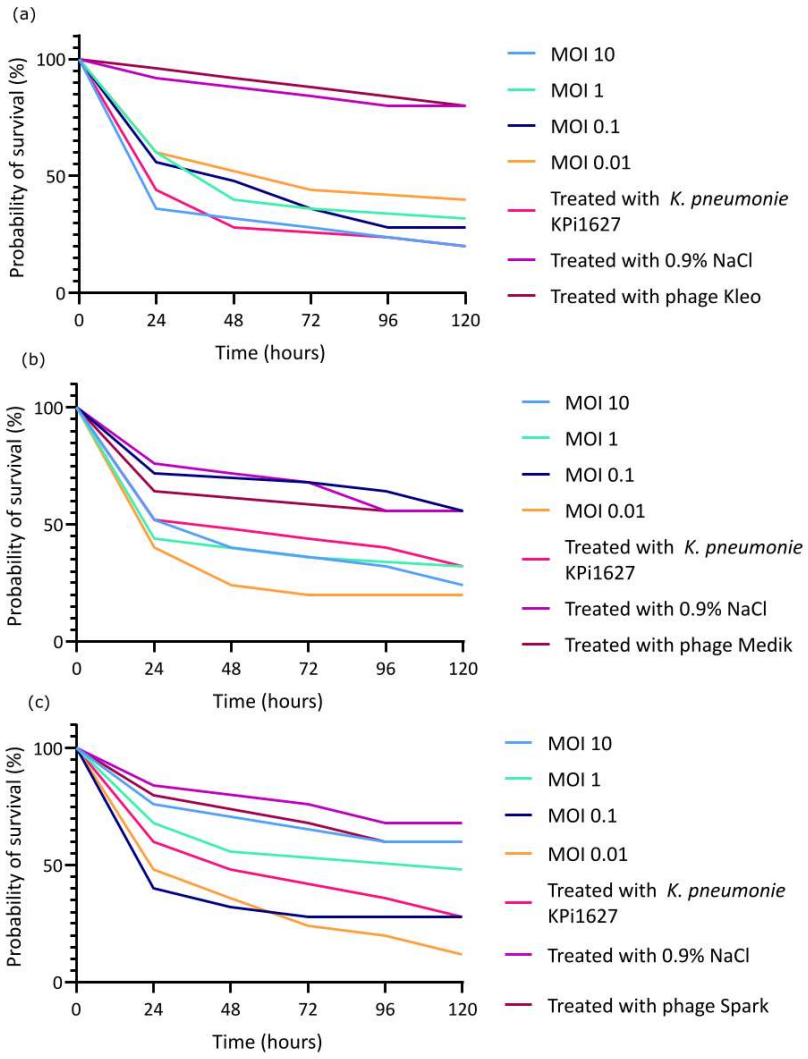



**Figure 5.** Survival of *Galleria mellonella* larvae infected with *Klebsiella pneumoniae* KPi1627 and treated with (**a**) Kleo, (**b**) Medik, or (**c**) Spark (top, middle, and bottom panels, respectively). Phages were administered at MOIs of 10, 1, 0.1, and 0.01; bacteria-only (K+), saline, and phage-only controls are shown for each experiment. Larval survival was monitored for 120 h. Each panel represents one experimental series with 25 larvae per group. Survival curves were analyzed using the Kaplan–Meier method and compared using the log-rank (Mantel–Cox) test. Global comparisons across the four treatment groups and K+ yielded $p = 0.402$ for Kleo, $p = 0.0527$ for Medik, and $p = 0.0030$ for Spark. Pairwise comparisons were considered exploratory, with unadjusted $p$-values reported for all phages. The Holm-adjusted result is additionally reported for the Spark MOI 10 comparison with the bacteria-only control. For Spark, the MOI 10 versus K+ comparison yielded an unadjusted $p = 0.0228$ and a Holm-adjusted $p = 0.0912$ after correction for four dose-specific comparisons.

Overall, the survival response varied between experimental series and across MOI levels. The largest numerical increase in final survival relative to the corresponding infected control was observed for Spark at MOI 10; however, this difference did not remain statistically significant after adjustment for multiple comparisons. Given that each phage was evaluated in a single experimental series, the survival findings should be interpreted as exploratory.

### *3.7. Genome Organization and Taxonomic Placement of Kleo, Medik, and Spark*

The genomes of phages Kleo, Medik, and Spark were 48,034 bp (NCBI accession number PZ533465), 46,646 bp (PZ533467), and 46,874 bp (PZ533466) in length, respectively. Their G + C contents were 48.7%, 49.0%, and 48.8%, respectively. These values are approximately 8 percentage points lower than the average G + C content reported for *K. pneumoniae* genomes (~57.1%) [82]. All three genomes had a similar organization, with recognizable DNA-packaging, structural, lysis, and replication-associated regions (Figure 6).

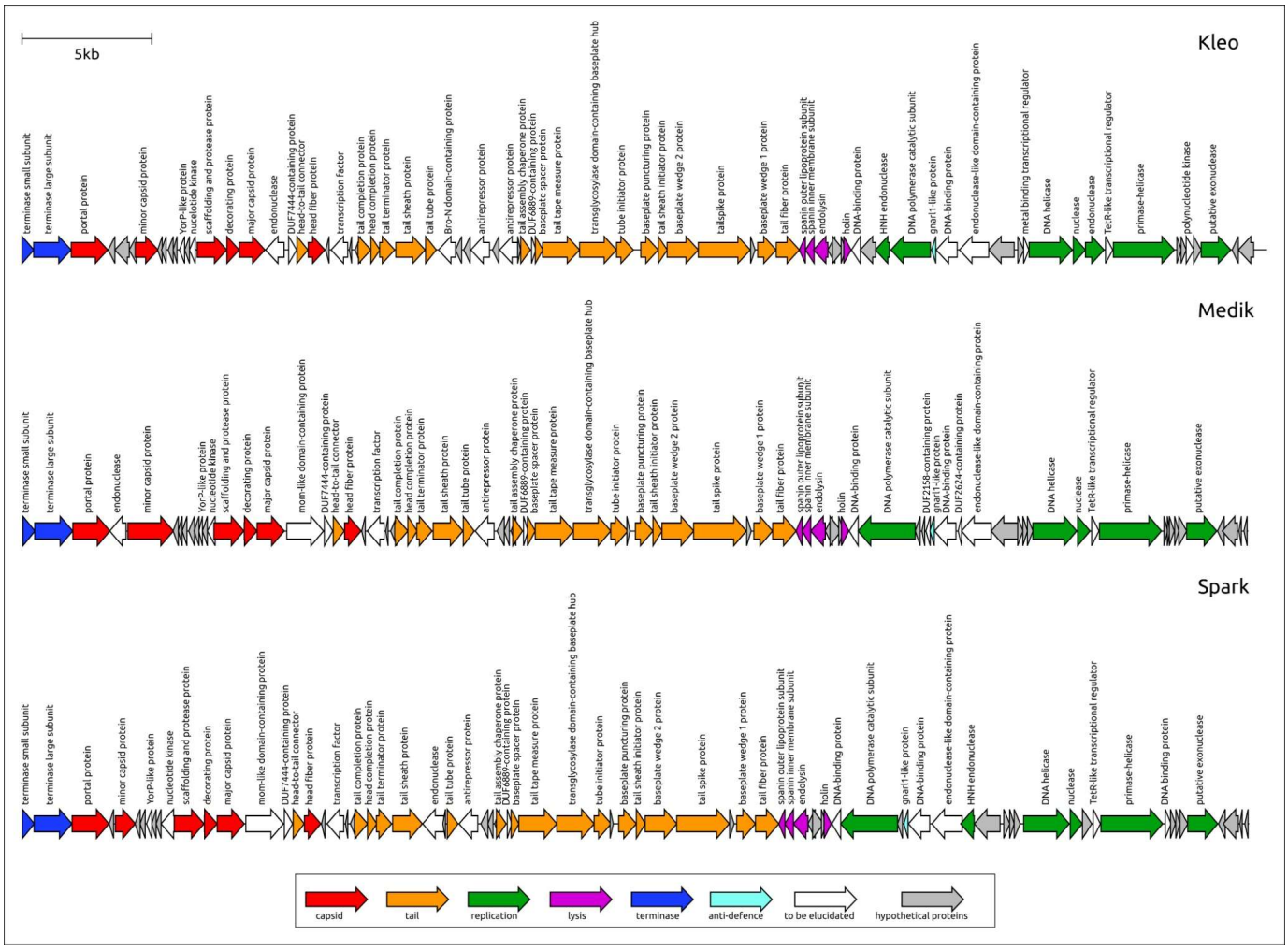



**Figure 6.** Genetic maps of phages Kleo, Medik, and Spark. Gene annotations and predicted functions are indicated by labels and the legend. Arrows indicate the direction of transcription. The scale bar represents genome length.

No matches to known virulence-factor genes were detected by searches against the VFDB core dataset under the conditions described in Materials and Methods. No integrase or C-type repressor genes were identified in the genome annotations.

VIRIDIC analysis showed that the closest classified relatives of Kleo, Medik, and Spark belong to the subfamily *Jameshumphriesvirinae* and the genus *Sircambvirus* (Figure 7). The closest classified relative of Kleo was *Klebsiella* phage vB_KpnM_FZ14 (*Sircambvirus FZ14*), with an intergenomic similarity of 76.2%. For Medik and Spark, the closest classified relative was *Klebsiella* phage vB_KpnM_KpV52 (*Sircambvirus KpV52*), with intergenomic similarities of 85.7% and 91.3%, respectively. Pairwise intergenomic similarities among Kleo, Medik, and Spark and between each phage and its closest classified relative were below

95% and above 70%. Using the commonly applied 95% species-level and 70% genus-level thresholds [58,83], the three phages therefore represent candidate members of three distinct species within the genus *Sircambvirus*.

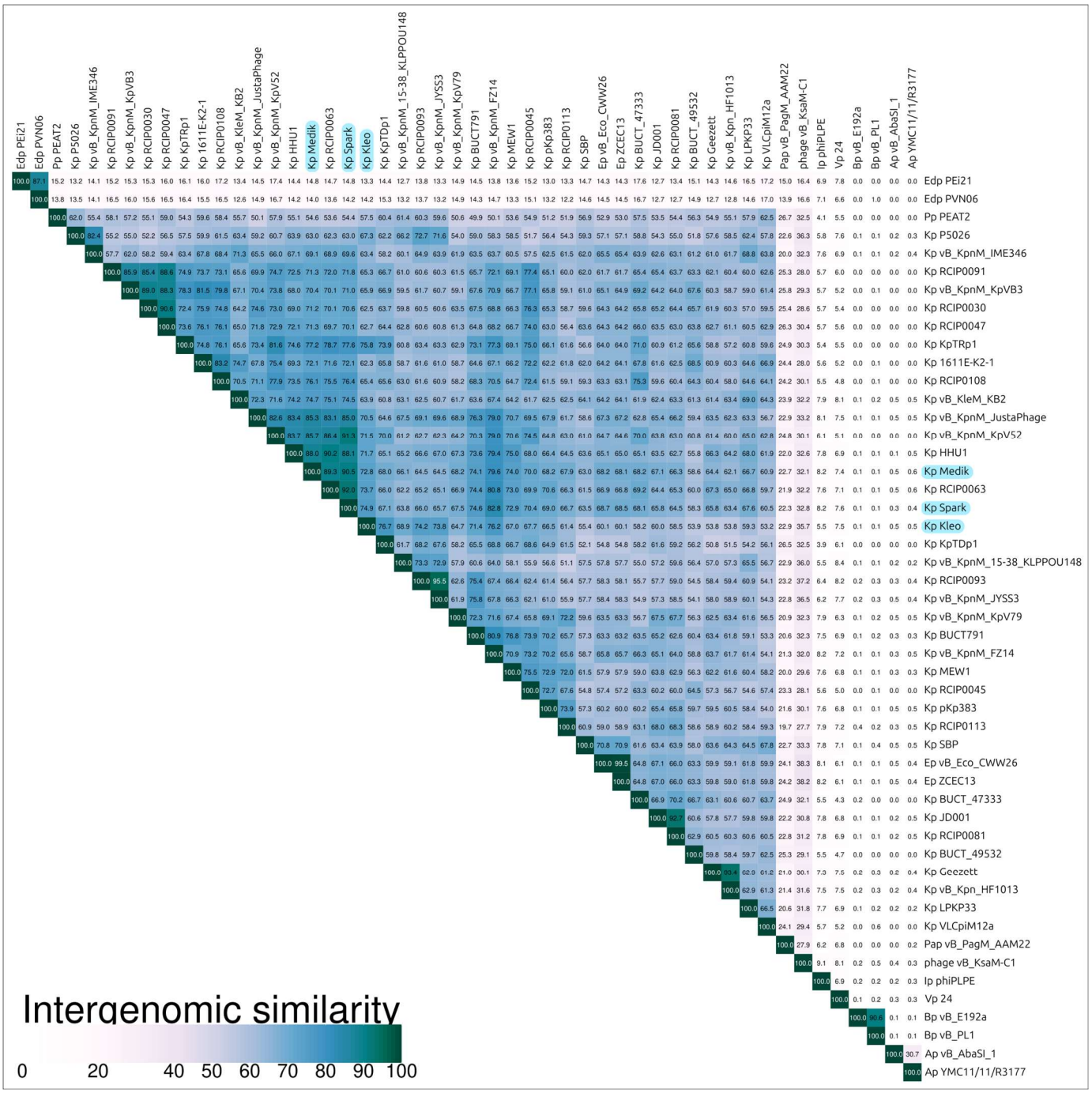
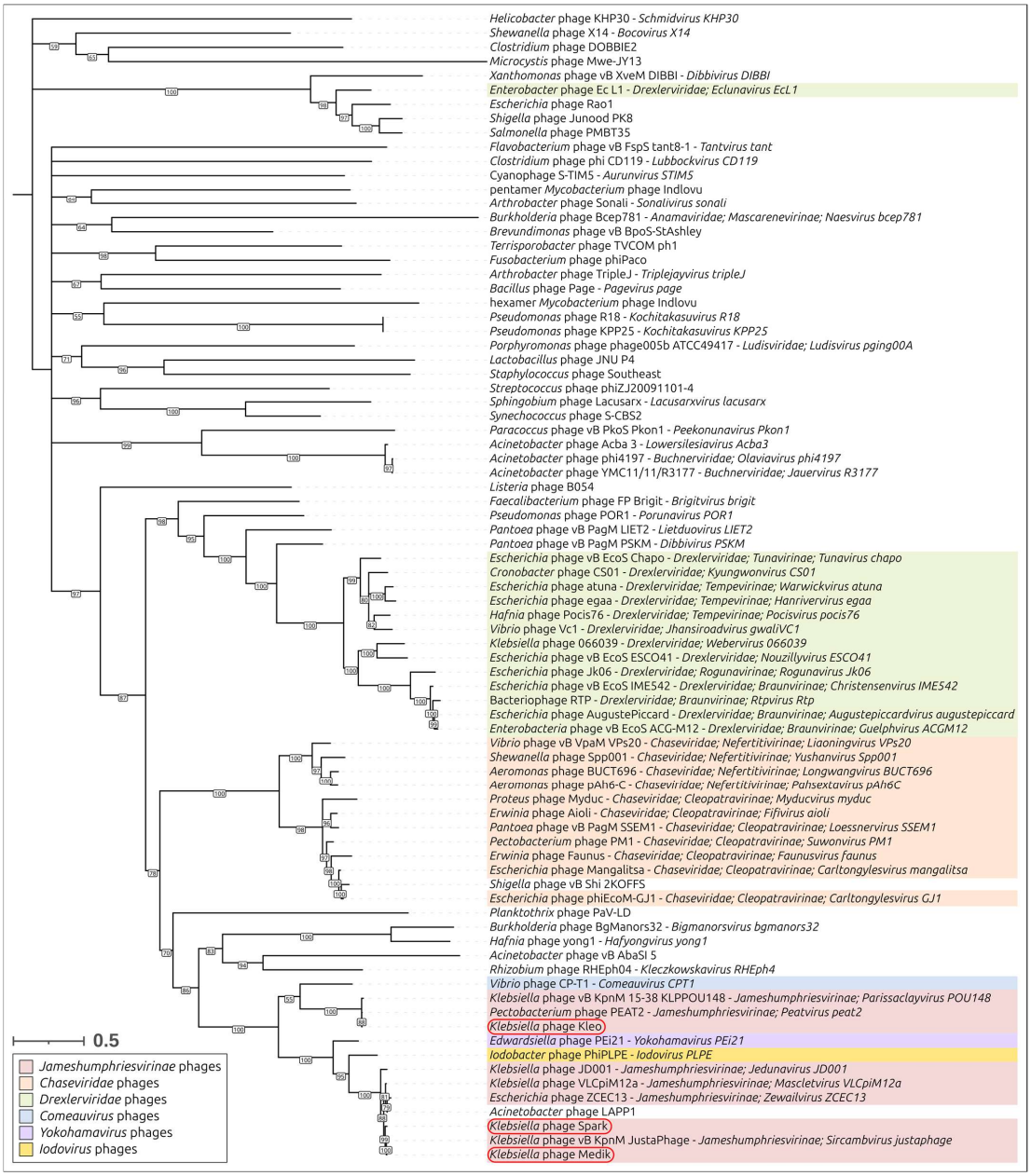



**Figure 7.** VIRIDIC heatmap of phages Kleo, Medik, Spark, and related phages identified by BLASTn searches against the GBPHG database. The dataset includes ICTV-classified representatives of the subfamily *Jameshumphriesvirinae*. Abbreviations: Edp, *Edwardsiella* phage; Pp, *Pectobacterium* phage; Kp, *Klebsiella* phage; Ep, *Escherichia* phage; Pap, *Pantoea* phage; Ip, *Iodobacter* phage; Vp, *Vibrio* phage; Bp, *Burkholderia* phage; Ap, *Acinetobacter* phage. The color gradient represents pairwise intergenomic similarity, ranging from 0% to 100%, as indicated by the color scale.

ViPTree analysis also placed Kleo, Medik, and Spark with members of *Sircambvirus* within the *Jameshumphriesvirinae* group (Supplementary Figure S1). In the VICTOR tree, all

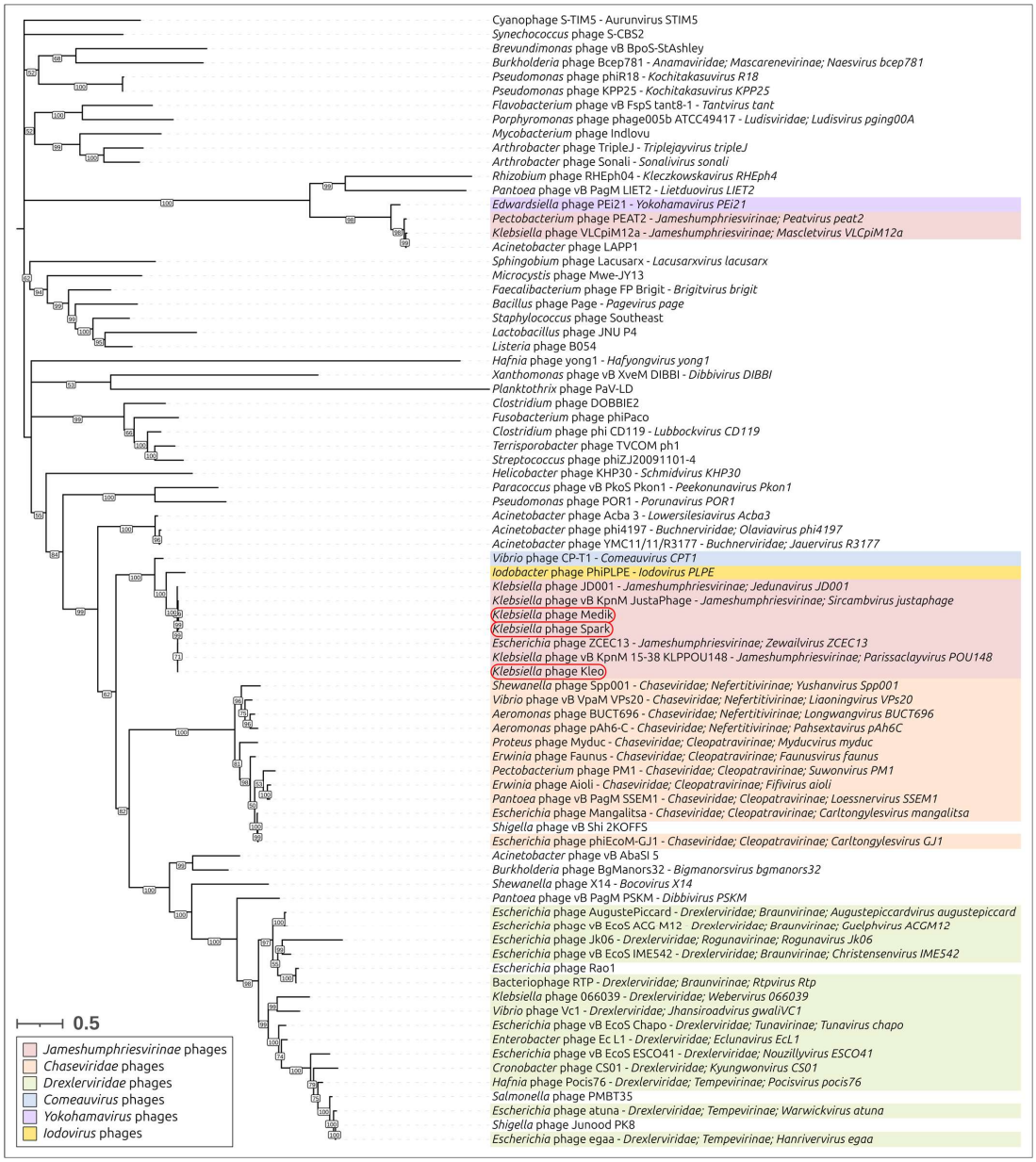
three phages remained within the *Jameshumphriesvirinae* clade; Medik and Spark grouped with *Sircambvirus* representatives, whereas Kleo occupied a separate position within the same broader clade (Supplementary Figure S2). These results support placement of Kleo, Medik, and Spark in the genus *Sircambvirus*.

To further examine the placement of Kleo, Medik, and Spark, maximum-likelihood trees were constructed for the major capsid protein (MCP) and the ATPase domain of the large terminase subunit (TLS) (Figure 8a,b). In both trees, the three phages clustered with representatives of the subfamily *Jameshumphriesvirinae*, although the broader topology differed between the two markers.




(**a**)

**Figure 8.** *Cont.*




(**b**)

**Figure 8.** Maximum-likelihood phylogenetic trees based on (**a**) major capsid protein (MCP) sequences and (**b**) ATPase-domain sequences of the large terminase subunit (TLS). Taxonomic assignments are indicated in the labels and legend. Branches with bootstrap support below 50% were collapsed; bootstrap values are shown near the corresponding branches. Trees were midpoint-rooted for visualization only; root positions were not used to infer ancestral relationships. Red outlines highlight the positions of phages Kleo, Medik, and Spark.

In the MCP tree, the sampled *Jameshumphriesvirinae* formed a single clade that also included *Acinetobacter* phage LAPP1 and representatives of the genera *Comeauvirus*, *Iodovirus*, and *Yokohamavirus*. In the TLS tree, *Jameshumphriesvirinae* representatives were divided between two groups: Kleo, Medik, and Spark clustered with one of them together with members of *Comeauvirus* and *Iodovirus*, whereas the second group was associated with *Yokohamavirus* and phage LAPP1. Both marker trees placed Kleo, Medik, and Spark within the broader *Jameshumphriesvirinae*-associated assemblage; their proposed assignment to *Sircambvirus* was supported by the whole-genome comparisons.

More distantly related representatives of the families *Chaseviridae* and *Drexlerviridae* formed separate groups in both analyses. The *Chaseviridae* clade also included the unclassified *Shigella* phage vB_Shi_2KOFFS. Most sampled *Drexlerviridae* grouped together in both trees, although *Enterobacter* phage Ec_L1 occupied a separate position in the MCP tree, and several unclassified phages were included in the corresponding TLS clade.

### *3.8. Whole-Genome and Gene-Sharing Network Structure of the Combined Phage Dataset*

The combined dataset of 452 phage genomes was analyzed using whole-genome nucleotide similarity and gene-sharing approaches (Figure 9a–d). At a tANI threshold of 0.95, Vclust complete-linkage clustering resolved the dataset into 323 operational species-level clusters, 272 of which were singletons. The largest species-level cluster contained 16 genomes. At a tANI threshold of 0.70, 149 operational genus-level clusters were obtained, including 112 singletons; the largest cluster comprised 173 genomes.

Kleo, Medik, and Spark belonged to three different species-level clusters. At the genus-level threshold, Medik and Spark were assigned to the same complete-linkage cluster, whereas Kleo was assigned to a different cluster. Pairwise tANI values were approximately 0.718 for Kleo–Medik, 0.740 for Kleo–Spark, and 0.901 for Medik–Spark.

The complete user-only vConTACT3 graph at identity layer 0.3 contained 36,049 gene-sharing edges. Of these, 16,011 (44.41%) connected genomes were assigned to the same Vclust genus-level complete-linkage cluster, whereas 20,038 (55.59%) connected genomes were assigned to different clusters. Thus, at this identity layer, gene-sharing relationships extended extensively across the boundaries of the operational genus-level groups defined by whole-genome nucleotide similarity.

### *3.9. Genomic Context and Phylogenomic Structure of Jameshumphriesvirinae*

To provide a broader genomic context for the phages examined in this study, genome-size distributions were compared for the complete *Caudoviricetes* dataset and for the subset of phages reported to infect *Klebsiella pneumoniae* (Figure 10a,b). Both distributions showed a major peak at approximately 40–60 kb and a smaller peak around 160–180 kb. The 46.6–48.0 kb genomes of Kleo, Medik, and Spark fall within the major genome-size range observed in both datasets.

Proteome-wide analysis with ViPTree was used to examine the relationships surrounding *Jameshumphriesvirinae*. In the 114-genome ViPTree analysis, 54 phages formed a clade containing the ICTV-classified members of *Jameshumphriesvirinae* included in the dataset (Supplementary Figure S3). Of these 54 phages, 36 were treated as putative members of the subfamily, including Kleo, Medik, and Spark. The same 54 phages also formed a distinct group in the VIRIDIC analysis (Supplementary Figure S4).

The MCP tree, based on 140 protein sequences, showed a more complex arrangement (Figure 11a). All 54 phages were located within a broader clade of 77 phages, but did not form a single monophyletic group. Instead, they were distributed between two subclades containing 48 and 6 phages. MCPs in the smaller subclade were 328–330 amino acids long, whereas those in the larger subclade were 344–348 amino acids long. The length difference was localized to the N-terminal region. Because the corresponding AlphaFold 3 predictions had low pLDDT scores, the structural basis of this difference was not interpreted further.

The TLS ATPase-domain tree, based on 332 sequences, showed a different arrangement (Figure 11b). The same 54 phages were distributed between two more distantly related clades containing 36 and 18 representatives, respectively, with ICTV-classified members of *Jameshumphriesvirinae* present in both. No representatives of the families *Lindbergviridae* or *Hirszfeldviridae* were recovered in the MCP homology search, whereas numerous representatives of both families were identified in the TLS search.

In the ViPTree, MCP, and TLS trees, representatives of *Iodovirus* (Iodobacteriophage phiPLPE), *Yokohamavirus* (*Edwardsiella* phages PEi21 and MSW-3), and *Comeauvirus* (*Vibrio* phages CP-T1 and vB_VchM-138) were consistently found within broader groups that also contained members of *Jameshumphriesvirinae*. At the same time, the internal distribution of the *Jameshumphriesvirinae*-associated phages differed markedly between the MCP- and TLS-based trees.

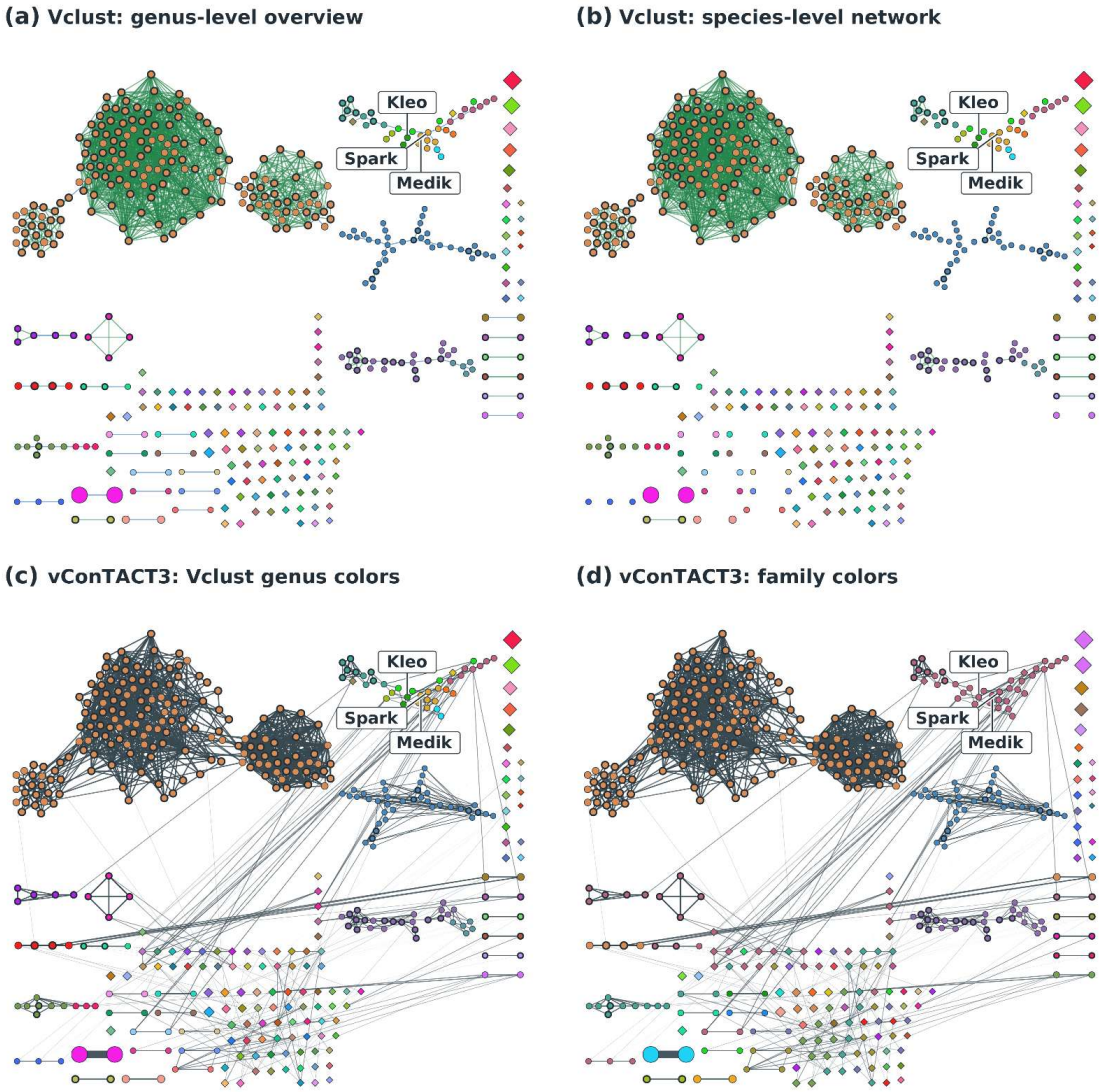



**Figure 9.** Network comparison of the combined dataset of 452 phage genomes. (**a**) Vclust overview showing all pairwise relationships with tANI ≥ 0.70. Nodes are colored according to complete-linkage genus-level clusters; green edges indicate species-level relationships (tANI ≥ 0.95), whereas blue edges indicate 0.70 ≤ tANI < 0.95. (**b**) Vclust species-level network showing all relationships with tANI ≥ 0.95 using the same node coordinates. (**c**) Sparsified vConTACT3 gene-sharing network derived from the complete identity-layer 0.3 graph for visualization as described in Materials and Methods; nodes are colored according to Vclust genus-level clusters. Edge width represents the number of shared protein clusters, and edge opacity represents 1 − SqRoot distance. (**d**) The same sparsified vConTACT3 network with nodes colored according to predicted family-level assignments. Node size is proportional to genome length. Circles indicate members of multi-genome genus-level clusters, diamonds indicate genus-level singletons, and thick node borders indicate membership in multi-genome species-level clusters. Node coordinates are preserved across panels to facilitate direct comparison. Quantitative gene-sharing statistics reported in the text were calculated from the complete vConTACT3 graph rather than from the sparsified network shown here.

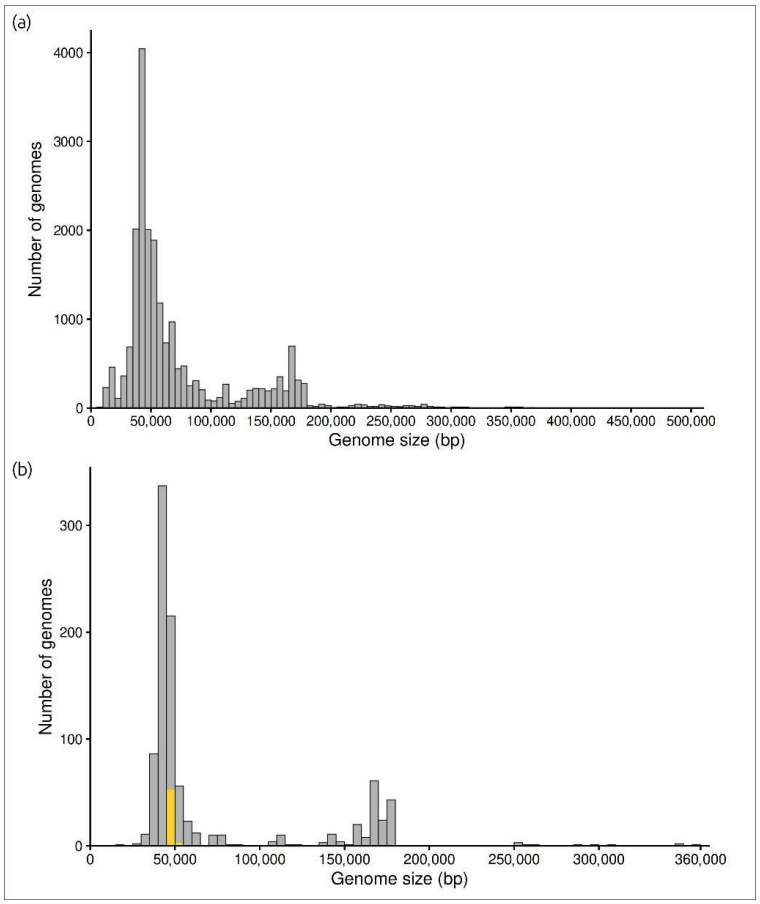



**Figure 10.** Distribution of genome sizes among tailed phage genomes. (**a**) Distribution of genome sizes in the analyzed *Caudoviricetes* dataset ($n$ = 20,659). (**b**) Distribution of genome sizes in the analyzed *Klebsiella pneumoniae* phage dataset ($n$ = 968). Yellow bars indicate genomes assigned in this study to the *Jameshumphriesvirinae*-associated group.

### *3.10. Structural and Evolutionary Analysis of Capsule-Specific Tailspike Proteins*

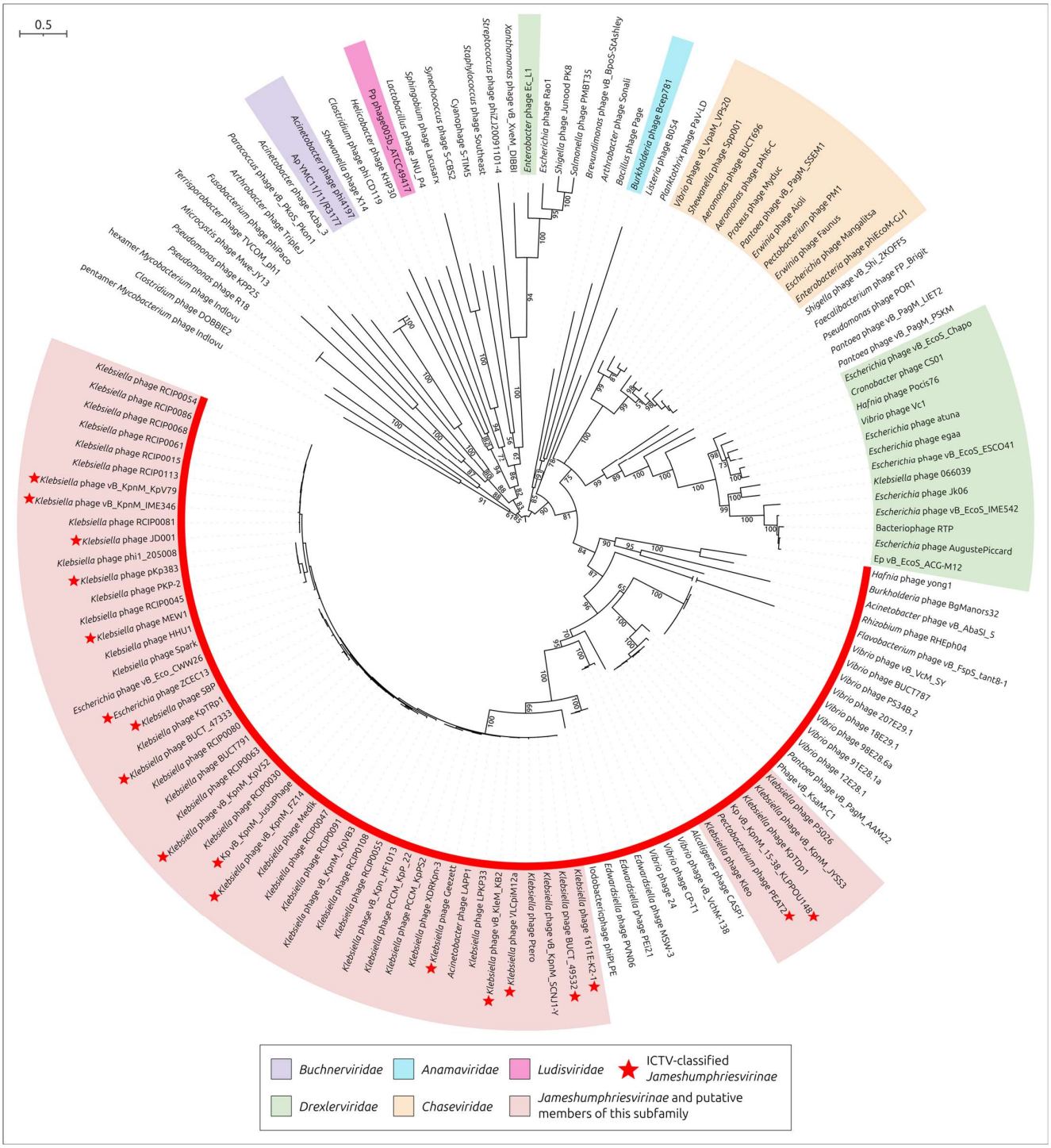
The TSP CDSs of Kleo, Medik, and Spark were identical in length (2007 nt, including the terminal stop codon) and encoded proteins of 668 amino acids; their global alignment yielded no gaps. Kleo and Medik differed at 41 positions, Kleo and Spark at only 8, and Medik and Spark at 40, corresponding to sequence identities of 97.96%, 99.60%, and 98.01%, respectively (Table 2). Notably, Kleo and Spark differed by only two amino acid residues, located at positions 40 and 50 in the N-terminal region, whereas their depolymerase regions were identical.

**Table 2.** Pairwise sequence identity of the TSPs and the median nucleotide identity of the other 48 single-copy homologous CDSs.

| Phage Pair | TSP Nucleotide Identity (%) | TSP Amino Acid Identity (%) | Other CDSs, Median Nucleotide Identity (%) |
|---|---|---|---|
| Kleo–Medik | 97.96 | 97.75 | 93.13 |
| Kleo–Spark | 99.60 | 99.70 | 93.23 |
| Medik–Spark | 98.01 | 97.46 | 98.90 |

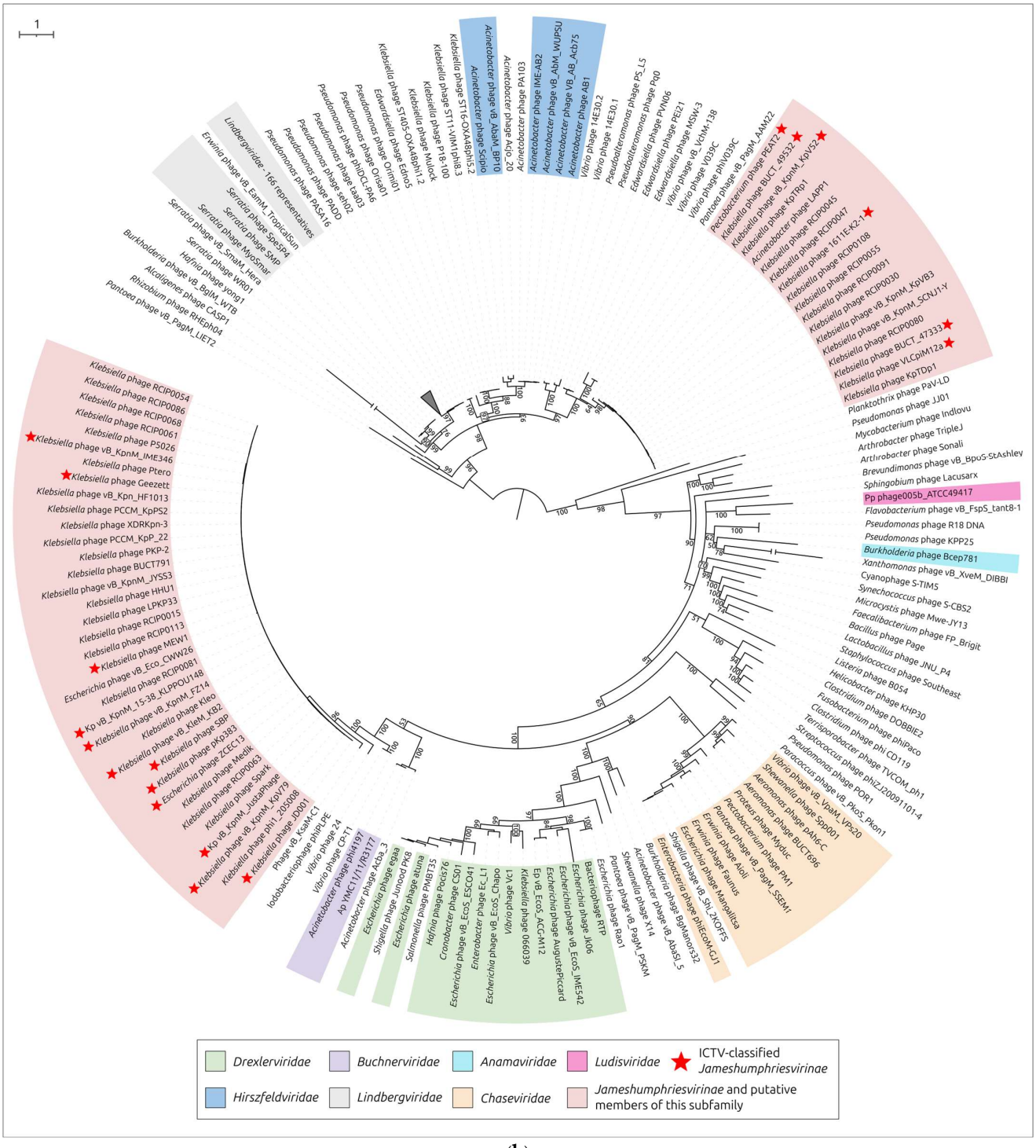
To place this high TSP similarity in the context of overall genomic relatedness, we compared the annotated proteomes of the three phages. This analysis identified 49 single-copy homologous groups shared by all three phages, one of which corresponded to the TSP.

Across the remaining 48 CDSs, the median nucleotide identity was 93.13% for Kleo–Medik, 93.23% for Kleo–Spark, and 98.90% for Medik–Spark (Table 2). Thus, TSP nucleotide identity was substantially higher than the median across the other 48 single-copy homologous CDSs in both comparisons involving Kleo. This difference was most pronounced for Kleo–Spark, for which the TSP showed 99.60% nucleotide identity compared with a median of 93.23% across the other shared CDSs and ranked third highest among the 49 homologous genes.




(**a**)

**Figure 11.** *Cont.*




(**b**)

**Figure 11.** Maximum-likelihood phylogenetic trees based on (**a**) major capsid protein (MCP) sequences and (**b**) ATPase-domain sequences of the large terminase subunit (TLS). Taxonomic assignments are indicated in the legend. Branches with bootstrap support below 50% are collapsed; bootstrap values are indicated near the corresponding branches. Trees were midpoint-rooted for visualization only; root positions were not used to infer ancestral relationships. Abbreviations: Ap, *Acinetobacter* phage; Ep, *Enterobacteria* phage; Kp, *Klebsiella* phage; Pp, *Porphyromonas* phage. In panel (**b**), a clade comprising 166 representatives of the family *Lindbergviridae*, predominantly members of the genus *Pbunavirus*, was collapsed and is represented by a triangle. Background colors indicate the corresponding taxonomic groups as specified in the legend. Red stars mark ICTV-classified members of *Jameshumphriesvirinae*.

The search against DepoCat, the catalog of *Klebsiella* phage experimentally characterized depolymerases, identified ORF16 of *Klebsiella* phage 1611E-K2-1 (*Bimevirus bv1611EK21*, subfamily *Jameshumphriesvirinae*), as the closest homolog with 88.2–88.5% amino acid identity to the three TSPs [67]. Recombinant ORF16 has been shown to degrade K2 CPS [84]. The AlphaFold 3 models of the Kleo, Medik, and Spark TSPs had the same overall fold as the ORF16 model and corresponded to DepoCat subclass 1B, characterized by a classical depolymerase architecture with a pouf-like C-terminal domain (Supplementary Figure S5).

The catalytic site has not been established for these TSPs. Their models contain conserved Asp355, Glu358, and Glu414 residues forming a negatively charged cavity at the interchain interface, which is a candidate polysaccharide-interacting site (Figure 12). The same residues are conserved in the more distant homologs with 40–45% identities within depolymerase regions: K2-degrading gp22 of *Klebsiella* phage NPat (*Webervirus NPat*, family *Drexlerviridae*) [85] and K2/K13-degrading DSCZNTNU_CDS0009 of Klebsiella phage KLEO13 (*Przondovirus*, family *Autotranscriptaviridae*) [67]. The tail spike protein gp196 of *Klebsiella* phage vB_KpM_FBKp24 (*Maaswegvirus Kp24*, family *Chimalliviridae*), which possesses the same activity against K2 and K13 [67,86], has an Asp residue substituted by Asn at the corresponding position in this candidate site.

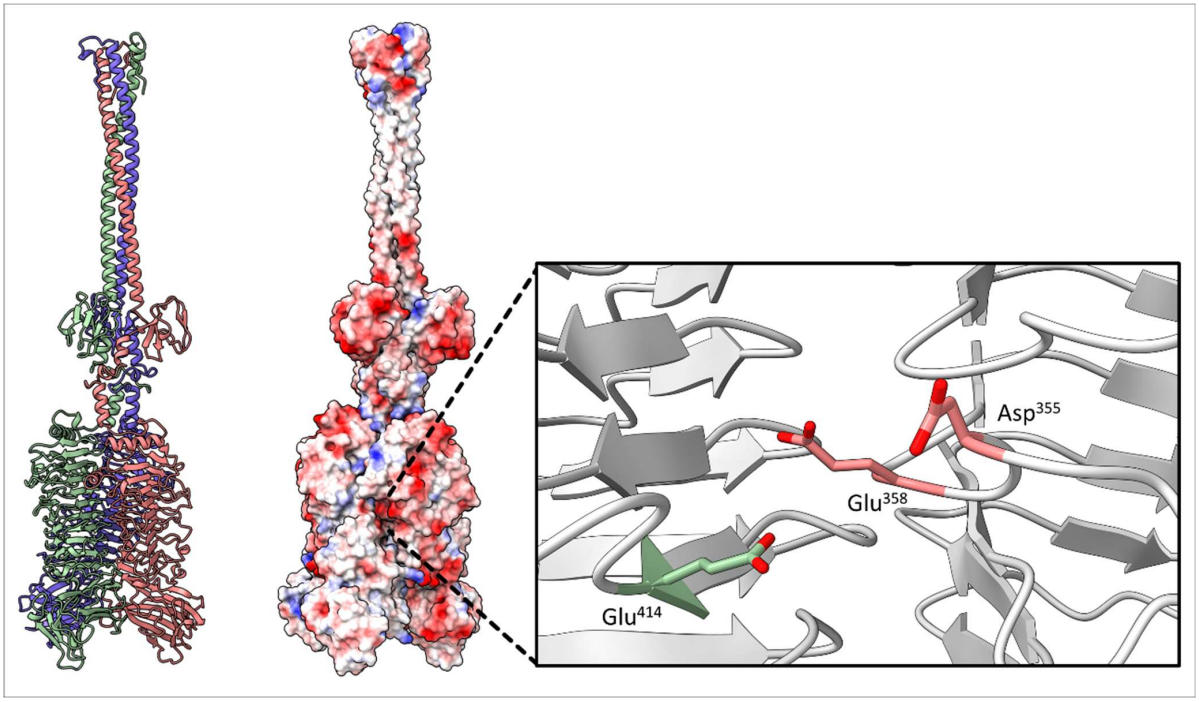
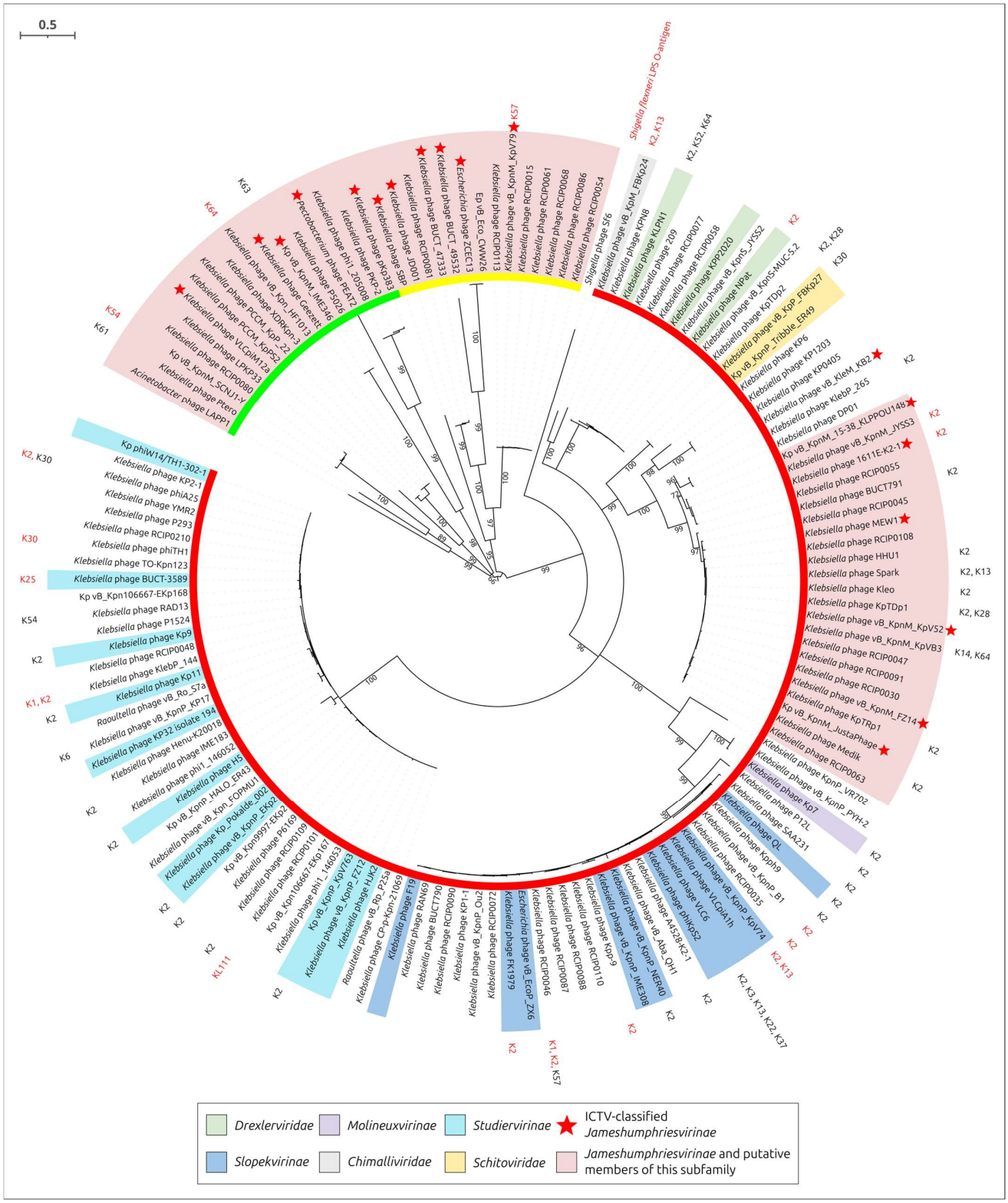



**Figure 12.** AlphaFold 3 model of the trimeric tailspike protein of *Klebsiella* phage Kleo. (**Left**), ribbon representation with the three monomers colored red, green, and blue. (**Center**), electrostatic surface representation, with negative regions in red and positive regions in blue. (**Right**), enlarged view of a candidate polysaccharide-interacting cavity at an interchain interface; residues from the two monomers are colored green and red, respectively.

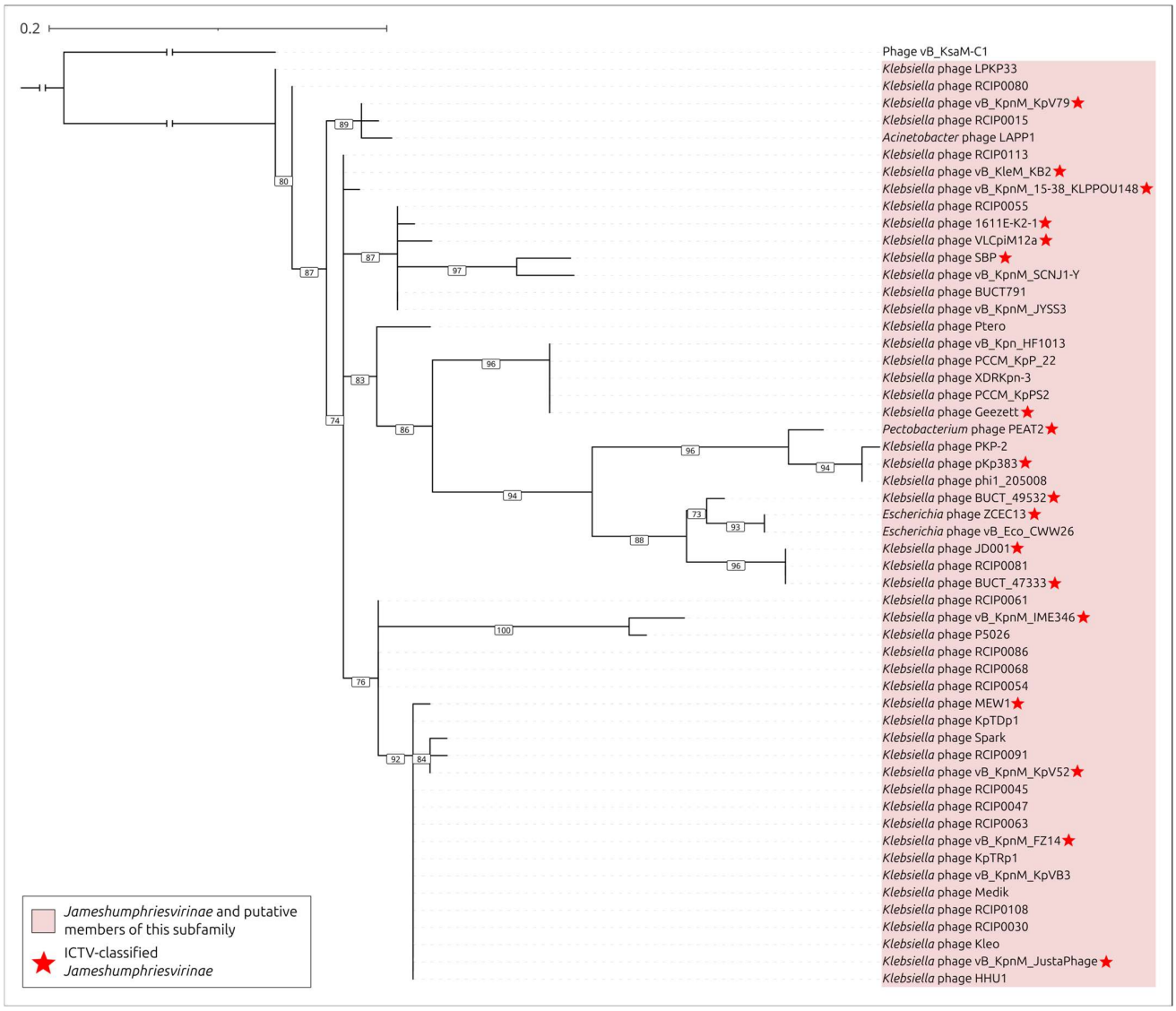
The phylogenetic tree based on the C-terminal depolymerase-containing region alignment comprised 142 proteins from phages belonging to different families and subfamilies (Figure 13a). In most of these phages, the proteins included in the tree were annotated as tailspike proteins. The taxa represented in the tree encompass different morphotypes: *Jameshumphriesvirinae* and *Chimalliviridae* are represented by myoviruses, *Drexlerviridae* by siphoviruses, and *Slopekvirinae*, *Molineuxvirinae*, *Studiervirinae*, and *Schitoviridae* by podoviruses. A large clade (indicated by a red arc) can be distinguished in the tree and

contains most of the phages included in the depolymerase-region dataset. Based on available data on phage hosts and experimental characterization of depolymerase activity, host capsule types were annotated next to the corresponding phages in the tree.




(**a**)

**Figure 13.** *Cont.*




(**b**)

**Figure 13.** Maximum-likelihood phylogenetic trees based on amino acid sequences of proteins representing different phages. (**a**) Depolymerase region-based phylogenetic tree. (**b**) N-terminal region-based phylogenetic tree. Taxonomic assignments are indicated in the legend. Branches with bootstrap support below 50% were collapsed. Bootstrap values are shown near their branches. Trees were midpoint-rooted for visualization only; root positions were not used to infer ancestral relationships. Capsule types are indicated next to the corresponding phage names. Red text indicates capsule types for which depolymerase activity has been experimentally demonstrated, whereas black text indicates capsule types assigned based on data for the corresponding phage hosts. Abbreviations are as follows: Ep—*Escherichia* phage; Kp—*Klebsiella* phage. The red, yellow, and green arcs indicate the three groups of *Jameshumphriesvirinae*-associated phages discussed in the Results. Background colors indicate taxonomic groups according to the legend.

Several subclades can be distinguished within the large clade, comprising representatives of *Drexlerviridae*, *Jameshumphriesvirinae*, *Slopekvirinae*, and *Studiervirinae*, together with individual phages representing *Molineuxvirinae*, *Chimalliviridae*, and *Schitoviridae*. For many phages within this large clade, available data indicate an association with the K2 capsule type. Interestingly, the TSP of *Shigella* phage Sf6, for which activity against the *Shigella flexneri* LPS O-antigen has been experimentally demonstrated [87–90], is positioned as a sister lineage to the large clade.

Overall, the 54 *Jameshumphriesvirinae*-associated phages identified in the proteome-wide analysis are distributed across the depolymerase-region tree in three groups. One of these groups forms a distinct subclade within the large clade together with representatives of other families and subfamilies. Phages Kleo, Medik, and Spark belong to this group. The other two groups (indicated by yellow and green arcs) consist exclusively of phages in the *Jameshumphriesvirinae*-associated group.

In the N-terminal-region tree, all phages except vB_KsaM-C1 were ICTV-classified members of *Jameshumphriesvirinae* or belonged to the putative *Jameshumphriesvirinae*-associated group (Figure 13b). Under the search conditions used, N-terminal homologs therefore had a much narrower taxonomic distribution than homologs of the depolymerase-containing region.

### *3.11. Synteny and Recombination Signals*

Of 1431 pairwise comparisons among the 54 genome records, 365 met the alignment-coverage criteria. All retained the internal order and relative orientation of matched CDSs after accounting for sequence-origin differences. The median fraction of conserved immediate gene adjacencies was 63.8% (interquartile range, 58.3–70.2%). The comparative maps illustrate this conserved organization together with variable local nucleotide similarity (Supplementary Figures S6 and S7). In several comparisons, nucleotide similarity was retained in the 5′ portion of the TSP gene, encoding the N-terminal part of the protein, whereas little or no similarity was detectable across the remainder of the gene. This pattern is consistent with conservation of the N-terminal attachment region and greater variability of the downstream region associated with capsule recognition and specificity.

GARD selected models with two to four breakpoints, dividing the five TSP alignments into three to five segments (Figure 14A–E). In the vB_KleM_KB2 group, boundaries after columns 119, 137, and 298 were retained after adding Kleo, Spark, and Medik (Figure 14A,B). The additional boundary after column 565 in the six-sequence group reduced AICc by only 1.01, indicating similar support for the three- and four-breakpoint models. The RCIP0080 group had boundaries after columns 144, 164, 730, and 766 (Figure 14C). The 12-sequence Ptero group had boundaries after columns 83, 150, 307, and 701, whereas the expanded 18-sequence Ptero selection had boundaries after columns 154 and 333 (Figure 14D,E). The two Ptero selections were assembled and aligned independently. All selected models favored segment-specific topologies over a common topology with the same partitions and independent branch lengths (ΔAICc = 34.03–989.74; Supplementary File S1).

The nine-sequence alignment of the expanded vB_KleM_KB2 group showed a pronounced change in local similarity involving BUCT791. Its residues 1–119 were identical to RCIP0055 but differed from Kleo at 14 positions. In contrast, residues 299–668 differed from Kleo and Spark at only one position and from RCIP0055 at 38 positions. Kleo and Spark differed only at residues 40 and 50. Medik differed from Kleo at 15 positions, including ten within residues 138–298; six of these differences were concentrated at residues 277–283.

RDP5 analysis yielded 12, 10, 10, and 38 candidate recombination signals in the Kleo, Spark, Medik, and 54-sequence datasets, respectively. The Spark and Medik alignments were identical, so their results did not constitute independent confirmation. In the 25-sequence dataset, a signal in Medik at CDS positions 815–896 (genomic positions 26,347–26,428; codons 272–299) was supported by six methods, although the right breakpoint remained imprecise.

Within this interval, Medik was more similar to RCIP0093 than to RCIP0108 (98.78% versus 80.49% nucleotide identity). Outside the interval, RCIP0108 was the closer match, with 97.81% identity compared with 83.82% for RCIP0093. A similar interval, CDS positions 815–893, was detected in the 54-sequence dataset, although the recombinant assignment

was flagged as uncertain. In JustaPhage, the CDS interval 752–928 was recovered in both the search-derived and 54-sequence datasets, although the inferred parental representatives differed.

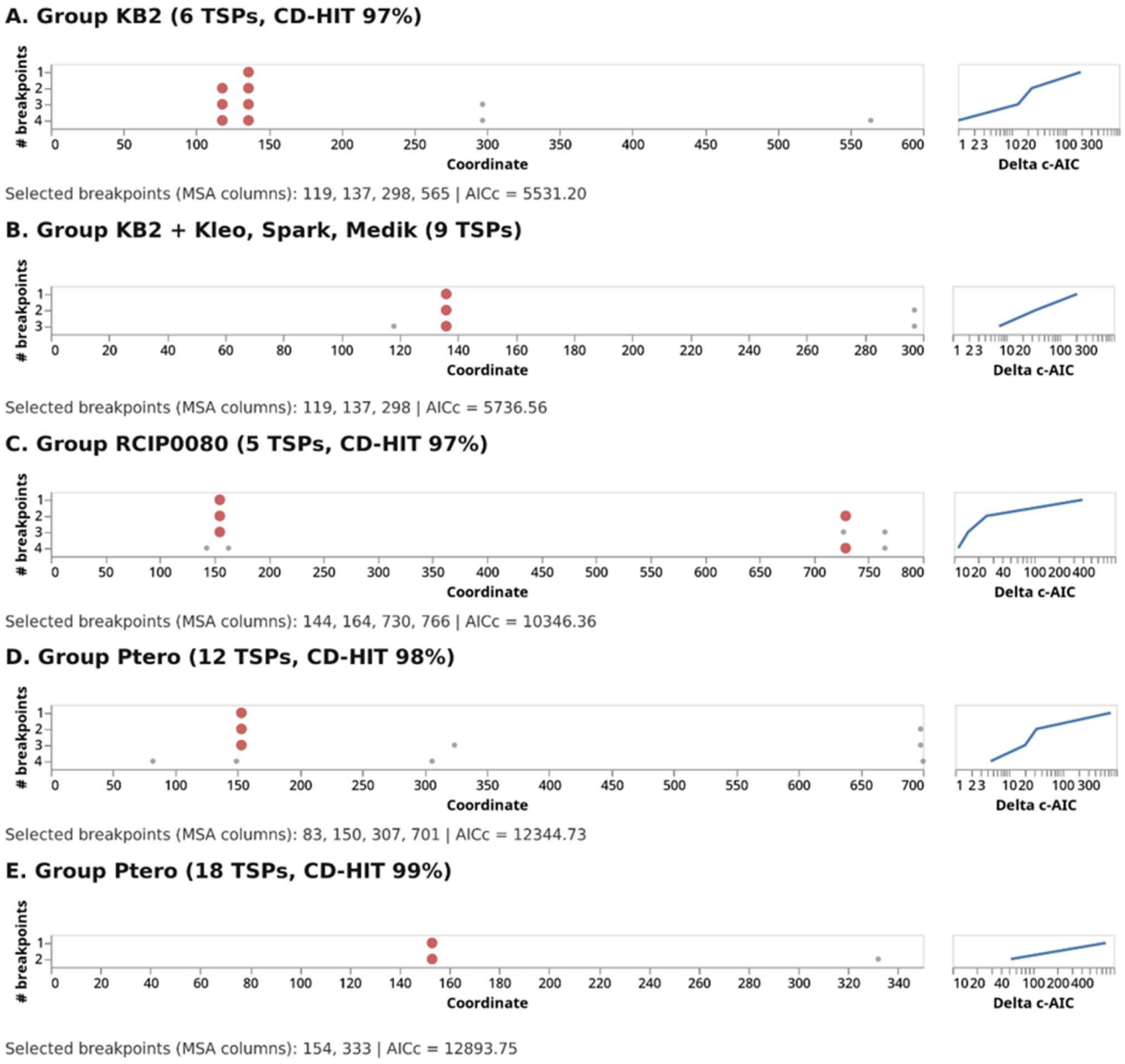



**Figure 14.** GARD analysis of five TSP amino acid datasets. (**A**) vB_KleM_KB2, abbreviated KB2 in the figure (six sequences; CD-HIT 97%). (**B**) The same group supplemented with Kleo, Spark, and Medik (nine sequences). (**C**) RCIP0080 (five sequences; 97%). (**D**) Ptero (12 sequences; 98%). (**E**) Expanded Ptero selection (18 sequences; 99%). Left plots show breakpoint configurations as the number of breakpoints increases. Larger red markers indicate persistence across model sizes, not statistical significance. Smaller gray markers indicate candidate breakpoints that are not consistently retained across the evaluated model sizes. Blue curves show the AICc reduction from the preceding model on a logarithmic scale.

## 4. Discussion

### *4.1. Biological Properties and Antibacterial Activity*

Kleo, Medik, and Spark add three experimentally characterized isolates to the K2-targeting phages of *Sircambvirus*. All three formed plaques surrounded by halos and were

active against both K2 strains in the test panel. Halo formation is commonly associated with phage-encoded polysaccharide depolymerases [78,79], and the similarity of their TSPs to the experimentally characterized K2-degrading ORF16 provides a molecular basis for this phenotype. Their activity against K2 strains is consistent with that reported for KpTRp1 and other K2-targeting phages [23,24,28,91]. In addition to their activity against K2 strains, the three phages exhibited different levels of activity against the KL13 isolate M190. Spark showed detectable activity with a relatively low EOP, whereas Kleo and Medik produced only rare plaques at high phage concentrations, with EOP values on the order of $10^{-8}$. Such extremely low values should be interpreted cautiously, as they do not establish efficient productive infection or substantial susceptibility of M190 to these phages. The structural similarity between K2 and K13 capsular polysaccharides provides a relevant context for this cross-reactivity [92]. Several K2-associated phage depolymerases, including Kpv74_56, K2-2, and B1dep, have been reported to exhibit cross-reactivity with K2 and K13 CPS [17,20,67]. However, depolymerase cross-reactivity does not necessarily imply productive infection of the corresponding phage. For example, B1dep degraded K13 CPS, whereas the B1 phage itself did not infect or lyse the K13 strain [20,67]. Thus, the observed activity of Kleo, Medik, and Spark against M190 is consistent with the documented K2/K13 cross-reactivity of some *Klebsiella* phage depolymerases, although the mechanism underlying this interaction remains to be established.

Kleo, Medik, and Spark showed rapid decreases in recoverable infectious phage titers following incubation with *K. pneumoniae* KPi1627, with the recoverable fraction reaching low levels within approximately 3–5 min. The assay was performed in the presence of $MgCl_2$ and $CaCl_2$, which can facilitate phage attachment [14,38,39], and used a chloroform-based sample-processing approach with a published methodological precedent [41]. These observations are consistent with rapid phage–host interactions under the experimental conditions. However, because the measured fraction was defined by recovery after chloroform treatment, the calculated apparent adsorption values should not be interpreted as direct measurements of irreversible attachment. The initial MOI of 0.0001, which yielded the highest final phage titers within the tested range, was comparable to the optimal MOI reported for the K2-specific *Sircambvirus* phage KpTRp1 [28]. Despite this similarity, the reproductive characteristics differed among K2-targeting phages. For KpTRp1, a latent period of approximately 30 min and a burst size of about 6 PFU per infected cell have been reported [28]. In our experiments, the first detectable increase in the titers of Kleo, Medik, and Spark occurred between 10 and 20 min after the operationally defined post-adsorption time zero, rather than after the onset of infection. The corresponding apparent burst-size estimates, calculated from the first post-rise plateau relative to the titer at time zero, were $27.5 \pm 3.7$, $45.3 \pm 4.5$, and $37.3 \pm 6.3$, respectively. These estimates depend on the assay design and should not be interpreted as independently validated measurements of progeny production per infected cell. For context, burst sizes of 25 and approximately 26 PFU per cell and latent periods of 11 and 15 min have been reported for the K2-targeting phages Kpph9 and vB_KlebPS_265, respectively [23,91]. However, differences in experimental procedures, definitions of time zero, and calculation methods limit direct quantitative comparison with our estimates. In contrast, the K2-specific phage HHU1 showed a substantially larger burst size of $134.17 \pm 33.81$ PFU per cell with a latent period of 10 min [24]. Thus, K2-targeting phages can exhibit markedly different reproductive characteristics despite their shared capsule specificity, highlighting the importance of characterizing individual phages separately.

Activity was also retained against established biofilms. Kleo, Medik, and Spark reduced crystal violet-stainable biomass by up to 75.8%, 61.9%, and 59.6%, respectively, extending the observations of antibiofilm activity in other *K. pneumoniae* phages [93,94]. However,

because crystal violet staining measures total attached biofilm biomass rather than bacterial viability, these reductions cannot be interpreted as direct evidence of bacterial killing within the biofilm. The largest reductions occurred at nominal input MOIs of 0.1, 0.01, and 0.001, respectively. These profiles differed from the common low-MOI maximum in the overnight propagation assay. Phage amplification in a growing culture and removal of biomass from a preformed biofilm therefore showed different dependencies on the initial phage input.

The results show that phage treatment did not produce the same survival response under all experimental conditions. The most pronounced effect was observed for Spark at MOI 10, where final survival increased from 28% in the infected control to 60%. At lower MOIs, however, this effect was not reproduced, suggesting that the outcome depended on the treatment conditions rather than simply on the presence of phage.

Such variability has also been reported in previous *G. mellonella* phage-therapy studies. Seed and Dennis showed that therapeutic efficacy against *Burkholderia cenocepacia* depended on both the phage dose and the timing of treatment. Importantly, phage DC1 failed to protect infected larvae across MOIs from 10 to 0.0001 despite high bacterial susceptibility to this phage in vitro. This demonstrates that strong in vitro activity does not necessarily result in improved survival in the larval model [95].

A similar observation was reported by Antoine et al. for phage PEV2 against *Pseudomonas aeruginosa*. Treatment over a wide MOI range (50–50,000) did not significantly improve larval survival. Nevertheless, at the higher MOIs, phage titers increased and bacterial titers were reduced at 24 and 48 h. Thus, the absence of a significant survival effect does not necessarily mean that a phage has no biological activity in vivo [96].

The numerical increase in larval survival observed for Spark at MOI 10 suggests a possible condition-dependent effect. However, this difference did not remain statistically significant after adjustment for multiple comparisons (Holm-adjusted $p = 0.0912$). Given that each phage was evaluated in a single experimental series, these findings should be interpreted as exploratory and require independent validation.

### *4.2. Genomic Relationships and Evolutionary Histories of Virion Components*

Kleo, Medik, and Spark had similar genome sizes, conserved gene organization, and related proteomes, but represented candidate members of three distinct *Sircambvirus* species according to the commonly used nucleotide similarity criteria [58,83]. Medik and Spark were the closest pair in the whole-genome comparison, whereas Kleo was more divergent. At a broader scale, gene-sharing relationships extended beyond nucleotide-defined groups: 20,038 of the 36,049 edges (55.59%) in the complete user-only vConTACT3 graph at identity layer 0.3 connected different operational genus-level clusters. Such connections reflect a distribution of homologous proteins that is broader than the groups defined by similarity across the genomes.

This organization is consistent with Botstein's model of modular phage evolution, in which exchange of genetic units produces genomes whose components have different evolutionary histories [29]. In the present dataset, patterns consistent with such mosaicism were observed even among phages that formed a coherent group in the proteome-wide analysis. The 54 *Jameshumphriesvirinae*-associated phages were divided into groups of 48 and 6 in the MCP tree, but into groups of 36 and 18 in the TLS ATPase-domain tree. The capsid and DNA-packaging components therefore retained different patterns of relatedness within the same set of genomes. The TLS homology search also recovered numerous representatives of *Lindbergviridae* and *Hirszfeldviridae*, whereas representatives of these families were absent from the MCP dataset. The different distributions of these two proteins are consistent with partly separate histories of capsid and packaging genes during the diversification of these phages.

The recurring relationships with *Iodovirus*, *Yokohamavirus*, and *Comeauvirus* further broaden the evolutionary context of *Jameshumphriesvirinae*. Representatives of these genera occurred near *Jameshumphriesvirinae*-associated phages in the proteome-wide, MCP, and TLS analyses, while relationships within this assemblage changed between the two protein trees. These results describe a group of related genomes whose morphogenesis components have not all followed the same evolutionary path. Genetic exchange among the lineages offers an explanation for the combination of conserved genome organization with different capsid and terminase relationships.

### *4.3. Modular Evolution of Tailspike Proteins*

The TSP comparison localized this evolutionary heterogeneity to a gene involved in recognition of the bacterial surface. Medik and Spark were the closest pair at the whole-genome level, but the most similar TSP sequences belonged to Kleo and Spark. Their TSP CDSs shared 99.60% nucleotide identity, compared with a median of 93.23% for the other 48 single-copy homologous genes. Kleo–Medik TSP identity also exceeded the corresponding median, whereas Medik–Spark TSP identity was slightly below it. The unusually close relationship of the Kleo and Spark TSP loci suggests a more recent shared history of this region than of most of their other shared genes. Exchange of a TSP-containing DNA segment is a plausible explanation for this localized similarity.

The TSPs also connect the biological properties of these isolates with the broader evolution of capsule recognition. Their closest characterized homolog, ORF16 of phage 1611E-K2-1, degrades K2 CPS, and the predicted proteins share its overall architecture. The candidate interchain cavity contains residues corresponding to those in more distant K2-active depolymerases from phages with different tail morphologies. These similarities associate the focal TSPs with a conserved polysaccharide-interacting architecture that occurs in otherwise different virions.

The phylogenies of the two TSP regions revealed a second level of modularity within the proteins themselves. Homologs of the N-terminal region were concentrated in *Jameshumphriesvirinae*-associated phages, whereas homologs of the depolymerase-containing region occurred in several families and subfamilies with contractile, long non-contractile, and short tails. This distribution suggests that the N-terminal attachment region has remained more closely associated with a particular virion assembly context, while the capsule-interacting region has had a broader evolutionary distribution. The 54 associated phages occupied three groups in the depolymerase-region tree, one of which also included homologs from other families and contained Kleo, Medik, and Spark. The diversity of these regions therefore exceeds the divisions visible in the whole-genome comparison.

Experimental exchanges of receptor-binding modules provide a functional basis for this interpretation. Latka et al. combined N-terminal attachment and C-terminal specificity modules from *Klebsiella* phage RBPs; the resulting chimeric proteins retained the capsule specificity of their C-terminal modules, and replacement of an RBP altered phage capsule serotype specificity [12,97]. Related mosaic organization has been described for *Escherichia coli* phage tailspikes, in which receptor-binding subtypes correlate with O-antigen serogroups across several phage genera [98]. Retention of an attachment module compatible with the virion, together with exchange of a polysaccharide-recognition module, provides a mechanism by which host-surface interactions can change without replacement of the entire tail apparatus.

The relationship to the TSP of *Shigella* phage Sf6 extends this comparison beyond capsular substrates. Sf6 TSP, an experimentally characterized enzyme acting on the *Shigella flexneri* LPS O-antigen [87], formed a sister lineage to the large depolymerase-region clade containing many K2-associated phages. Thus, homologous polysaccharide-recognition

architectures occur in proteins acting on different components of the bacterial surface. In the phages examined here, the different histories of whole genomes, morphogenesis proteins, and regions within TSPs are consistent with modular exchange operating at both genomic and intragenic levels.

### *4.4. Recombination Signals and Shared Ancestry*

The TSP comparisons revealed changes in sequence relationships along individual genes. In BUCT791, residues 1–119 were identical to those of RCIP0055, whereas residues 299–668 differed from Kleo and Spark at only one position. Thus, different parts of the same TSP had their closest sequence matches in different relatives. Together with the phylogenetic partitions identified by GARD, this pattern supports recombination among related tailspike genes.

A similar change in local sequence relationships occurred within the Medik TSP gene. Outside the candidate interval at CDS positions 815–896, Medik was more similar to RCIP0108 than to RCIP0093; within this interval, the relationship was reversed. RDP5 identified a recombination signal in this region, which overlaps codons 272–299 and includes six amino acid differences from Kleo concentrated at residues 277–283. The localized signal is therefore accompanied by a change in the closest nucleotide sequence match and a concentration of amino acid differences.

These observations extend the comparison of the N-terminal and depolymerase-containing regions described above. The broader phylogenies associated these major regions with different sets of phage lineages. The BUCT791 and Medik comparisons reveal a finer pattern of mosaicism among closely related TSPs, involving long regions with different sequence relationships and a short internal tract. Local exchange among related genes therefore offers an additional mechanism of tailspike diversification alongside the reassortment of major protein regions.

## 5. Conclusions

Kleo, Medik, and Spark are candidate members of three distinct *Sircambvirus* species. Under the experimental conditions tested, all three phages exhibited rapid adsorption-associated decreases in recoverable infectious titers and reduced crystal violet-stainable biomass of preformed biofilms. The *Galleria mellonella* experiments revealed differences in larval survival among treatment conditions; however, these findings should be regarded as exploratory because each phage was evaluated in a single experimental series. Their evolutionary relationships varied between whole genomes and individual components. Gene-sharing links connected nucleotide-defined groups, and capsid and terminase phylogenies divided the same proteomically related phages differently. The close similarity of the Kleo and Spark TSP loci contrasted with the greater whole-genome similarity of Medik and Spark. Within TSPs, the N-terminal and depolymerase-containing regions had different taxonomic distributions. These findings support a mosaic evolutionary history involving both phage genes and functional regions within individual proteins.

**Supplementary Materials:** The following supporting information can be downloaded at: https://www.mdpi.com/article/10.3390/v18111279/s1, Figure S1: ViPTree proteomic tree of Kleo, Medik, Spark, and related dsDNA phages. Figure S2: VICTOR phylogenomic tree of Kleo, Medik, Spark, and related dsDNA phages. Figure S3: ViPTree proteomic analysis of the 114-genome dataset surrounding *Jameshumphriesvirinae*. Figure S4: VIRIDIC comparison of the *Jameshumphriesvirinae*-associated genome dataset. Figure S5: Comparison of the AlphaFold 3 model of the trimeric Kleo tailspike with *Klebsiella* depolymerases of known substrate specificity. Figure S6: MCP-oriented comparative genome map of the 54 *Jameshumphriesvirinae*-associated phages. Figure S7: MCP-oriented comparative genome map of the shared reference-phage set recovered by tBLASTn searches with the Kleo, Spark, and Medik TSPs.

All three searches retained the same 22 external homologues; their input datasets differed only in inclusion of the study phages. A single map is therefore shown, without separate query-specific panels. Table S1: Antimicrobial resistance determinants detected in *K. pneumoniae* M190. Table S2: Phenotypic antimicrobial susceptibility of *Klebsiella pneumoniae* M190 determined by disk diffusion, including inhibition zone diameters and EUCAST interpretations. Table S3: GenBank accession numbers and descriptions of the 452 phage genome records used in the whole-genome and gene-sharing network analyses. Table S4: Replicate-level plaque counts, phage dilutions, and corresponding reference-host titers used to calculate the efficiency of plating on *K. pneumoniae* M190. File S1. Input alignments and corresponding output files for the GARD and RDP5 recombination analyses.

**Author Contributions:** Conceptualization P.V.E.; methodology, P.V.E., A.A.V., L.I.I., A.V.C., K.S.T., G.A.S. and M.V.N.; software, A.V.C., P.V.E., M.A.Y., A.A.V. and M.V.N.; validation, A.A.V., M.V.N., A.V.C., P.V.E., G.A.S., K.S.T., M.A.Y. and V.A.K.; formal analysis, A.A.V., A.V.C., P.V.E., M.V.N. and L.I.I.; investigation, A.A.V., M.V.N., A.V.C., P.V.E., G.A.S., K.S.T., M.A.Y. and N.V.O.; resources, P.V.E.; data curation, A.A.V., M.V.N., A.V.C. and P.V.E.; writing—original draft preparation, A.A.V., M.V.N., A.V.C., P.V.E., and M.A.Y.; writing—review and editing, A.A.V., A.V.C. and P.V.E.; visualization, A.A.V., M.V.N., A.V.C., P.V.E. and N.V.O.; supervision P.V.E. and L.I.I.; project administration, P.V.E., L.I.I. and D.A.S.; funding acquisition, P.V.E., L.I.I. and D.A.S. All authors have read and agreed to the published version of the manuscript.

**Funding:** This study was supported by the Development Program of the Federal State Autonomous Educational Institution of Higher Education "N.I. Pirogov Russian National Research Medical University" of the Ministry of Health of the Russian Federation (Pirogov University), within the framework of the Priority 2030 program. No individual grant number was assigned to this support.

**Institutional Review Board Statement:** Publication of this manuscript was approved under clearance No. 18 dated 8 October 2026.

**Informed Consent Statement:** Not applicable.

**Data Availability Statement:** The genome accession numbers are PZ533465 for Kleo, PZ533467 for Medik, PZ533466 for Spark, and JCBHEB000000000 for *K. pneumoniae* M190 (NCBI GenBank). The accession numbers for the 452-genome comparative dataset are provided in Supplementary Table S3.

**Acknowledgments:** The authors gratefully acknowledge Nikolay V. Volozhantsev for providing the *Klebsiella pneumoniae* isolates used in this study.

**Conflicts of Interest:** The authors declare no conflicts of interest.

## References

1. Paczosa, M.K.; Mecsas, J. *Klebsiella pneumoniae*: Going on the Offense with a Strong Defense. *Microbiol. Mol. Biol. Rev.* **2016**, *80*, 629–661. [CrossRef] [PubMed]
2. WHO Bacterial Priority Pathogens List, 2024: Bacterial Pathogens of Public Health Importance to Guide Research, Development and Strategies to Prevent and Control Antimicrobial Resistance. Available online: https://www.who.int/publications/i/item/9789240093461 (accessed on 10 July 2026).
3. Antimicrobial Resistance in the EU/EEA (EARS-Net)—Annual Epidemiological Report for 2024. Available online: https://www.ecdc.europa.eu/en/publications-data/antimicrobial-resistance-eueea-ears-net-annual-epidemiological-report-2024 (accessed on 23 June 2026).
4. Russo, T.A.; Marr, C.M. Hypervirulent *Klebsiella pneumoniae*. *Clin. Microbiol. Rev.* **2019**, *32*, e00001-19. [CrossRef] [PubMed]
5. Zhu, J.; Wang, T.; Chen, L.; Du, H. Virulence Factors in Hypervirulent *Klebsiella pneumoniae*. *Front. Microbiol.* **2021**, *12*, 642484. [CrossRef] [PubMed]
6. Pristas, I.; Ujevic, J.; Bodulić, K.; Andrijasevic, N.; Bedenic, B.; Payerl-Pal, M.; Susic, E.; Dobrovic, K.; De Koster, S.; Malhotra-Kumar, S.; et al. The Association between Resistance and Virulence of *Klebsiella pneumoniae* in High-Risk Clonal Lineages ST86 and ST101. *Microorganisms* **2024**, *12*, 1997. [CrossRef] [PubMed]
7. Han, B.; Feng, C.; Jiang, Y.; Ye, C.; Wei, Y.; Liu, J.; Zeng, Z. Mobile Genetic Elements Encoding Antibiotic Resistance Genes and Virulence Genes in *Klebsiella pneumoniae*: Important Pathways for the Acquisition of Virulence and Resistance. *Front. Microbiol.* **2025**, *16*, 1529157. [CrossRef] [PubMed]

8. Majkowska-Skrobek, G.; Latka, A.; Berisio, R.; Squeglia, F.; Maciejewska, B.; Briers, Y.; Drulis-Kawa, Z. Phage-Borne Depolymerases Decrease *Klebsiella pneumoniae* Resistance to Innate Defense Mechanisms. *Front. Microbiol.* **2018**, *9*, 2517. [CrossRef] [PubMed]
9. Latka, A.; Maciejewska, B.; Majkowska-Skrobek, G.; Briers, Y.; Drulis-Kawa, Z. Bacteriophage-Encoded Virion-Associated Enzymes to Overcome the Carbohydrate Barriers during the Infection Process. *Appl. Microbiol. Biotechnol.* **2017**, *101*, 3103–3119. [CrossRef] [PubMed]
10. Townsend, E.M.; Kelly, L.; Gannon, L.; Muscatt, G.; Dunstan, R.; Michniewski, S.; Sapkota, H.; Kiljunen, S.J.; Kolsi, A.; Skurnik, M.; et al. Isolation and Characterization of Klebsiella Phages for Phage Therapy. *PHAGE* **2021**, *2*, 26–42. [CrossRef] [PubMed]
11. Gholizadeh, O.; Ghaleh, H.E.G.; Tat, M.; Ranjbar, R.; Dorostkar, R. The Potential Use of Bacteriophages as Antibacterial Agents against *Klebsiella pneumoniae*. *Virol. J.* **2024**, *21*, 191. [CrossRef] [PubMed]
12. Le Bris, J.; Chen, N.; Supandy, A.; Rendueles, O.; Van Tyne, D. Phage Therapy for *Klebsiella pneumoniae*: Understanding Bacteria-Phage Interactions for Therapeutic Innovations. *PLoS Pathog.* **2025**, *21*, e1012971. [CrossRef] [PubMed]
13. Ding, J.; Yan, W.; Zheng, R.; Ma, M.; Jiang, L. Combating *Klebsiella pneumoniae*: From Antimicrobial Resistance Mechanisms to Phage-Based Combination Therapies. *Front. Cell Infect. Microbiol.* **2025**, *15*, 1691215. [CrossRef] [PubMed]
14. Jamal, M.; Hussain, T.; Das, C.R.; Andleeb, S. Characterization of Siphoviridae Phage Z and Studying Its Efficacy against Multidrug-Resistant *Klebsiella pneumoniae* Planktonic Cells and Biofilm. *J. Med. Microbiol.* **2015**, *64*, 454–462. [CrossRef] [PubMed]
15. Zurabov, F.; Zhilenkov, E. Characterization of Four Virulent *Klebsiella pneumoniae* Bacteriophages, and Evaluation of Their Potential Use in Complex Phage Preparation. *Virol. J.* **2021**, *18*, 9. [CrossRef] [PubMed]
16. Jiao, X.; Wang, M.; Liu, Y.; Yang, S.; Yu, Q.; Qiao, J. Bacteriophage-Derived Depolymerase: A Review on Prospective Antibacterial Agents to Combat *Klebsiella pneumoniae*. *Arch. Virol.* **2025**, *170*, 70. [CrossRef] [PubMed]
17. Ye, T.-J.; Fung, K.-M.; Lee, I.-M.; Ko, T.-P.; Lin, C.-Y.; Wong, C.-L.; Tu, I.-F.; Huang, T.-Y.; Yang, F.-L.; Chang, Y.-P.; et al. *Klebsiella pneumoniae* K2 Capsular Polysaccharide Degradation by a Bacteriophage Depolymerase Does Not Require Trimer Formation. *mBio* **2024**, *15*, e03519-23. [CrossRef] [PubMed]
18. Solovieva, E.V.; Myakinina, V.P.; Kislichkina, A.A.; Krasilnikova, V.M.; Verevkin, V.V.; Mochalov, V.V.; Lev, A.I.; Fursova, N.K.; Volozhantsev, N.V. Comparative Genome Analysis of Novel Podoviruses Lytic for Hypermucoviscous *Klebsiella pneumoniae* of K1, K2, and K57 Capsular Types. *Virus Res.* **2018**, *243*, 10–18. [CrossRef] [PubMed]
19. Volozhantsev, N.V.; Borzilov, A.I.; Shpirt, A.M.; Krasilnikova, V.M.; Verevkin, V.V.; Denisenko, E.A.; Kombarova, T.I.; Shashkov, A.S.; Knirel, Y.A.; Dyatlov, I.A. Comparison of the Therapeutic Potential of Bacteriophage KpV74 and Phage-Derived Depolymerase (β-Glucosidase) against *Klebsiella pneumoniae* Capsular Type K2. *Virus Res.* **2022**, *322*, 198951. [CrossRef] [PubMed]
20. Pertics, B.Z.; Cox, A.; Nyúl, A.; Szamek, N.; Kovács, T.; Schneider, G. Isolation and Characterization of a Novel Lytic Bacteriophage against the K2 Capsule-Expressing Hypervirulent *Klebsiella pneumoniae* Strain 52145, and Identification of Its Functional Depolymerase. *Microorganisms* **2021**, *9*, 650. [CrossRef] [PubMed]
21. Rahimi, S.; Bakht, M.; Javadi, A.; Foroughi, F.; Marashi, S.M.A.; Nikkhahi, F. Characterization of Novel Bacteriophage PSKP16 and Its Therapeutic Potential against β-Lactamase and Biofilm Producer Strain of K2-Hypervirulent *Klebsiella pneumoniae* Pneumonia Infection in Mice Model. *BMC Microbiol.* **2023**, *23*, 233. [CrossRef] [PubMed]
22. Wang, M.; Liu, J.; Jiao, X.; Liu, Y.; Yang, S.; Gong, W.; Qiao, J. Isolation, Characterization, Therapeutic Potential and Depolymerase Identification of a Lytic Bacteriophage Kpp-9 against *Klebsiella pneumoniae* with Capsule Serotype K2. *Microb. Pathog.* **2025**, *208*, 107950. [CrossRef] [PubMed]
23. Yakubovskij, V.I.; Morozova, V.V.; Kozlova, Y.N.; Tikunov, A.Y.; Fedorets, V.A.; Zhirakovskaya, E.V.; Babkin, I.V.; Bardasheva, A.V.; Tikunova, N.V. Phage vB_KlebPS_265 Active Against Resistant/MDR and Hypermucoid K2 Strains of *Klebsiella pneumoniae*. *Viruses* **2025**, *17*, 83. [CrossRef] [PubMed]
24. Han, P.; Sun, S.; Wen, L.; Yang, L.; Li, E.; Yang, Y. Isolation, Characterization and Therapeutic Evaluation of Phage HHU1 against K2 *Klebsiella pneumoniae*. *Front. Cell. Infect. Microbiol.* **2025**, *15*, 1668727. [CrossRef] [PubMed]
25. Rollon, W.D.; Dean, T.D.; Idris, S.I.M.; Mazlan, N.; Jati, A.P.; Thung, T.Y. Characterization of a Virulent Phage, P12L (Genus Drulisvirus), Targeting *Klebsiella pneumoniae* Capsule Type K2. *Arch. Virol.* **2025**, *170*, 128. [CrossRef] [PubMed]
26. Ge, G.; Ge, H.; Xu, J.; Yue, B.; Yang, Q.; Cheng, Z.; Guo, Z.; Deng, H.; Hou, H.; Shi, S.; et al. Two Tail Protein-Derived Capsule Depolymerases from Phage vB_KpnS_GH-K1 Are Effective against Pneumonia Caused by K2 Serotype *Klebsiella pneumoniae*. *Int. J. Antimicrob. Agents* **2026**, *67*, 107662. [CrossRef] [PubMed]
27. Master Species Lists (MSL)|ICTV. Available online: https://ictv.global/msl (accessed on 7 October 2026).
28. Kazdaghli, R.; Mourali, D.; Mora-Quilis, L.; Domingo-Calap, P.; Ben-Mahrez, K. Isolation and Characterization of a Novel Phage Targeting *Klebsiella pneumoniae* K2 Capsular Type. *Braz. J. Microbiol.* **2025**, *56*, 1887–1900. [CrossRef] [PubMed]
29. Botstein, D. A Theory of Modular Evolution for Bacteriophages. *Ann. N. Y. Acad. Sci.* **1980**, *354*, 484–490. [CrossRef] [PubMed]
30. Adams, M.H. *Bacteriophages*; Interscience Publishers: New York, NY, USA, 1959.
31. Kutter, E. Phage Host Range and Efficiency of Plating. *Methods Mol. Biol.* **2009**, *501*, 141–149. [CrossRef] [PubMed]

32. Lukianova, A.A.; Shneider, M.M.; Tokmakova, A.D.; Landyshev, N.N.; Kasimova, A.A.; Kolganova, A.S.; Mikhailova, Y.V.; Shelenkov, A.A.; Dmitrenok, A.S.; Chizhov, A.O.; et al. Novel Autographivirales Phages Kiwi, Nika and Pie Targeting *Klebsiella pneumoniae* K14: Isolation, Characterisation, Genome Analysis and Study of the Bacterial Polysaccharide Degradation. *Arch. Virol.* **2026**, *171*, 64. [CrossRef] [PubMed]
33. Disk Diffusion and Quality Control. Available online: https://www.eucast.org/bacteria/methodology-and-instructions/disk-diffusion-and-quality-control/ (accessed on 8 July 2026).
34. Clinical Breakpoint Tables. Available online: https://www.eucast.org/bacteria/clinical-breakpoints-and-interpretation/clinical-breakpoint-tables/ (accessed on 8 July 2026).
35. Media Preparation. Available online: https://www.eucast.org/bacteria/methodology-and-instructions/media-preparation/ (accessed on 8 July 2026).
36. Kropinski, A.M. Practical Advice on the One-Step Growth Curve. In *Bacteriophages: Methods and Protocols*; Clokie, M.R.J., Kropinski, A.M., Lavigne, R., Eds.; Springer: New York, NY, USA, 2018; Volume 3, pp. 41–47, ISBN 978-1-4939-7343-9. [CrossRef] [PubMed]
37. Li, P.; Lin, H.; Mi, Z.; Xing, S.; Tong, Y.; Wang, J. Screening of Polyvalent Phage-Resistant Escherichia Coli Strains Based on Phage Receptor Analysis. *Front. Microbiol.* **2019**, *10*, 850. [CrossRef] [PubMed]
38. Nawaz, A.; Khalid, N.A.; Zaheer, S.; Khan, M.I.; Khalid, A.; Shah, A.A.; Badshah, M.; Khan, S. Isolation and Characterization of a Potent Bacteriophage KA Targeting an Antibiotic-Resistant Human Pathogenic Strain of *Klebsiella pneumoniae* KP1. *Microb. Pathog.* **2026**, *210*, 108150. [CrossRef] [PubMed]
39. Mohammadi, M.; Saffari, M.; Siadat, S.D.; Hejazi, S.H.; Shayestehpour, M.; Motallebi, M.; Eidi, M. Isolation, Characterization, Therapeutic Potency, and Genomic Analysis of a Novel Bacteriophage vB_KshKPC-M against Carbapenemase-Producing *Klebsiella pneumoniae* Strains (CRKP) Isolated from Ventilator-Associated Pneumoniae (VAP) Infection of COVID-19 Patients. *Ann. Clin. Microbiol. Antimicrob.* **2023**, *22*, 18. [CrossRef] [PubMed]
40. Troshin, K.; Sykilinda, N.; Shuraleva, S.; Tokmakova, A.; Tkachenko, N.; Kurochkina, L.; Miroshnikov, K.; Suzina, N.; Brzhozovskaya, E.; Petrova, K.; et al. Pseudomonas Phage Lydia and the Evolution of the Mesyanzhinovviridae Family. *Viruses* **2025**, *17*, 369. [CrossRef] [PubMed]
41. Nabergoj, D.; Modic, P.; Podgornik, A. Effect of Bacterial Growth Rate on Bacteriophage Population Growth Rate. *MicrobiologyOpen* **2018**, *7*, e00558. [CrossRef] [PubMed]
42. Kropinski, A.M. Measurement of the Rate of Attachment of Bacteriophage to Cells. In *Bacteriophages: Methods and Protocols, Volume 1: Isolation, Characterization, and Interactions*; Clokie, M.R.J., Kropinski, A.M., Eds.; Humana Press: Totowa, NJ, USA, 2009; pp. 151–155, ISBN 978-1-60327-164-6. [CrossRef] [PubMed]
43. Tsai, C.J.-Y.; Loh, J.M.S.; Proft, T. Galleria Mellonella Infection Models for the Study of Bacterial Diseases and for Antimicrobial Drug Testing. *Virulence* **2016**, *7*, 214–229. [CrossRef] [PubMed]
44. Wick, R.R.; Judd, L.M.; Gorrie, C.L.; Holt, K.E. Unicycler: Resolving Bacterial Genome Assemblies from Short and Long Sequencing Reads. *PLoS Comput. Biol.* **2017**, *13*, e1005595. [CrossRef] [PubMed]
45. Bouras, G.; Nepal, R.; Houtak, G.; Psaltis, A.J.; Wormald, P.-J.; Vreugde, S. Pharokka: A Fast Scalable Bacteriophage Annotation Tool. *Bioinformatics* **2022**, *39*, btac776. [CrossRef] [PubMed]
46. Söding, J.; Biegert, A.; Lupas, A.N. The HHpred interactive server for protein homology detection and structure prediction. *Nucleic Acids Res.* **2005**, *33*, W244. [CrossRef] [PubMed]
47. Holm, L. Dali Server: Structural Unification of Protein Families. *Nucleic Acids Res.* **2022**, *50*, W210–W215. [CrossRef] [PubMed]
48. Abramson, J.; Adler, J.; Dunger, J.; Evans, R.; Green, T.; Pritzel, A.; Ronneberger, O.; Willmore, L.; Ballard, A.J.; Bambrick, J.; et al. Accurate Structure Prediction of Biomolecular Interactions with AlphaFold 3. *Nature* **2024**, *630*, 493–500. [CrossRef] [PubMed]
49. Tesson, F.; Huiting, E.; Wei, L.; Ren, J.; Johnson, M.; Planel, R.; Cury, J.; Feng, Y.; Bondy-Denomy, J.; Bernheim, A. Exploring the Diversity of Anti-Defense Systems across Prokaryotes, Phages and Mobile Genetic Elements. *Nucleic Acids Res.* **2024**, *53*, gkae1171. [CrossRef] [PubMed]
50. Kolmogorov, M.; Yuan, J.; Lin, Y.; Pevzner, P.A. Assembly of Long, Error-Prone Reads Using Repeat Graphs. *Nat. Biotechnol.* **2019**, *37*, 540–546. [CrossRef] [PubMed]
51. Bouras, G.; Judd, L.M.; Edwards, R.A.; Vreugde, S.; Stinear, T.P.; Wick, R.R. How Low Can You Go? Short-Read Polishing of Oxford Nanopore Bacterial Genome Assemblies. *Microb. Genom.* **2024**, *10*, 001254. [CrossRef] [PubMed]
52. Lam, M.M.C.; Wick, R.R.; Watts, S.C.; Cerdeira, L.T.; Wyres, K.L.; Holt, K.E. A Genomic Surveillance Framework and Genotyping Tool for *Klebsiella pneumoniae* and Its Related Species Complex. *Nat. Commun.* **2021**, *12*, 4188. [CrossRef] [PubMed]
53. Wyres, K.L.; Wick, R.R.; Gorrie, C.; Jenney, A.; Follador, R.; Thomson, N.R.; Holt, K.E. Identification of Klebsiella Capsule Synthesis Loci from Whole Genome Data. *Microb. Genom.* **2016**, *2*, e000102. [CrossRef] [PubMed]

54. Carattoli, A.; Zankari, E.; García-Fernández, A.; Voldby Larsen, M.; Lund, O.; Villa, L.; Møller Aarestrup, F.; Hasman, H. In Silico Detection and Typing of Plasmids Using PlasmidFinder and Plasmid Multilocus Sequence Typing. *Antimicrob. Agents Chemother.* **2014**, *58*, 3895–3903. [CrossRef] [PubMed]
55. van den Belt, M.; Gilchrist, C.; Booth, T.J.; Chooi, Y.-H.; Medema, M.H.; Alanjary, M. CAGECAT: The CompArative GEne Cluster Analysis Toolbox for Rapid Search and Visualisation of Homologous Gene Clusters. *BMC Bioinform.* **2023**, *24*, 181. [CrossRef] [PubMed]
56. Gilchrist, C.L.M.; Chooi, Y.-H. Clinker & Clustermap.Js: Automatic Generation of Gene Cluster Comparison Figures. *Bioinformatics* **2021**, *37*, 2473–2475. [CrossRef] [PubMed]
57. Altschul, S.F.; Gish, W.; Miller, W.; Myers, E.W.; Lipman, D.J. Basic Local Alignment Search Tool. *J. Mol. Biol.* **1990**, *215*, 403–410. [CrossRef] [PubMed]
58. Moraru, C.; Varsani, A.; Kropinski, A.M. VIRIDIC—A Novel Tool to Calculate the Intergenomic Similarities of Prokaryote-Infecting Viruses. *Viruses* **2020**, *12*, 1268. [CrossRef] [PubMed]
59. Nishimura, Y.; Yoshida, T.; Kuronishi, M.; Uehara, H.; Ogata, H.; Goto, S. ViPTree: The Viral Proteomic Tree Server. *Bioinformatics* **2017**, *33*, 2379–2380. [CrossRef] [PubMed]
60. Meier-Kolthoff, J.P.; Göker, M. VICTOR: Genome-Based Phylogeny and Classification of Prokaryotic Viruses. *Bioinformatics* **2017**, *33*, 3396–3404. [CrossRef] [PubMed]
61. Katoh, K.; Standley, D.M. MAFFT Multiple Sequence Alignment Software Version 7: Improvements in Performance and Usability. *Mol. Biol. Evol.* **2013**, *30*, 772–780. [CrossRef] [PubMed]
62. Wong, T.K.F.; Ly-Trong, N.; Ren, H.; Demotte, P.; Baños, H.; Roger, A.J.; Susko, E.; Bielow, C.; De Maio, N.; Goldman, N.; et al. IQ-TREE 3: Phylogenomic Inference Software Using Complex Evolutionary Models. *Mol. Biol. Evol.* **2026**, *43*, msag117. [CrossRef] [PubMed]
63. Letunic, I.; Bork, P. Interactive Tree of Life (iTOL) v6: Recent Updates to the Phylogenetic Tree Display and Annotation Tool. *Nucleic Acids Res.* **2024**, *52*, W78–W82. [CrossRef] [PubMed]
64. Zhou, S.; Liu, B.; Zheng, D.; Chen, L.; Yang, J. VFDB 2025: An Integrated Resource for Exploring Anti-Virulence Compounds. *Nucleic Acids Res.* **2024**, *53*, D871–D877. [CrossRef] [PubMed]
65. Camargo, A.P.; Roux, S.; Schulz, F.; Babinski, M.; Xu, Y.; Hu, B.; Chain, P.S.G.; Nayfach, S.; Kyrpides, N.C. Identification of Mobile Genetic Elements with geNomad. *Nat. Biotechnol.* **2024**, *42*, 1303–1312. [CrossRef] [PubMed]
66. Peng, C.; Shang, J.; Guan, J.; Sun, Y. ViralQC: A Tool for Assessing Completeness and Contamination of Predicted Viral Contigs. *Bioinformatics* **2026**, *42*, btag463. [CrossRef] [PubMed]
67. Otwinowska, A.; Olejniczak, S.; Latka, A.; Pozniak, M.; Majkowska-Skrobek, G.; Maciejewska, B.; Koszucki, J.; Panicker, V.R.; Jablonska, S.; Hulsens, M.; et al. DepoCatalog: Mapping Diversity of 129 Recombinantly Produced Klebsiella Phage Depolymerases. *Nat. Commun.* **2026**, *17*, 6724. [CrossRef] [PubMed]
68. Zhang, C.; Shine, M.; Pyle, A.M.; Zhang, Y. US-Align: Universal Structure Alignments of Proteins, Nucleic Acids, and Macromolecular Complexes. *Nat. Methods* **2022**, *19*, 1109–1115. [CrossRef] [PubMed]
69. Cock, P.J.A.; Antao, T.; Chang, J.T.; Chapman, B.A.; Cox, C.J.; Dalke, A.; Friedberg, I.; Hamelryck, T.; Kauff, F.; Wilczynski, B.; et al. Biopython: Freely Available Python Tools for Computational Molecular Biology and Bioinformatics. *Bioinformatics* **2009**, *25*, 1422–1423. [CrossRef] [PubMed]
70. Zielezinski, A.; Gudyś, A.; Barylski, J.; Siminski, K.; Rozwalak, P.; Dutilh, B.E.; Deorowicz, S. Ultrafast and Accurate Sequence Alignment and Clustering of Viral Genomes. *Nat. Methods* **2025**, *22*, 1191–1194. [CrossRef] [PubMed]
71. Bolduc, B.; Zablocki, O.; Turner, D.; Bin Jang, H.; Guo, J.; Adriaenssens, E.M.; Dutilh, B.E.; Sullivan, M.B. Machine Learning Enables Scalable and Systematic Hierarchical Virus Taxonomy. *Nat. Biotechnol.* **2025**. [CrossRef] [PubMed]
72. Shannon, P.; Markiel, A.; Ozier, O.; Baliga, N.S.; Wang, J.T.; Ramage, D.; Amin, N.; Schwikowski, B.; Ideker, T. Cytoscape: A Software Environment for Integrated Models of Biomolecular Interaction Networks. *Genome Res.* **2003**, *13*, 2498–2504. [CrossRef] [PubMed]
73. Darling, A.E.; Mau, B.; Perna, N.T. progressiveMauve: Multiple Genome Alignment with Gene Gain, Loss and Rearrangement. *PLoS ONE* **2010**, *5*, e11147. [CrossRef] [PubMed]
74. Fu, L.; Niu, B.; Zhu, Z.; Wu, S.; Li, W. CD-HIT: Accelerated for Clustering the Next-Generation Sequencing Data. *Bioinformatics* **2012**, *28*, 3150–3152. [CrossRef] [PubMed]
75. Steinegger, M.; Söding, J. MMseqs2 Enables Sensitive Protein Sequence Searching for the Analysis of Massive Data Sets. *Nat. Biotechnol.* **2017**, *35*, 1026–1028. [CrossRef] [PubMed]
76. Kosakovsky Pond, S.L.; Posada, D.; Gravenor, M.B.; Woelk, C.H.; Frost, S.D.W. Automated Phylogenetic Detection of Recombination Using a Genetic Algorithm. *Mol. Biol. Evol.* **2006**, *23*, 1891–1901. [CrossRef] [PubMed]
77. Martin, D.P.; Varsani, A.; Roumagnac, P.; Botha, G.; Maslamoney, S.; Schwab, T.; Kelz, Z.; Kumar, V.; Murrell, B. RDP5: A Computer Program for Analyzing Recombination in, and Removing Signals of Recombination from, Nucleotide Sequence Datasets. *Virus Evol.* **2021**, *7*, veaa087. [CrossRef] [PubMed]

78. Abedon, S.T. Detection of Bacteriophages: Phage Plaques. In *Bacteriophages: Biology, Technology, Therapy*; Harper, D.R., Abedon, S.T., Burrowes, B.H., McConville, M.L., Eds.; Springer: Cham, Switzerland, 2021; pp. 507–538. [CrossRef]
79. Lukianova, A.A.; Shneider, M.M.; Evseev, P.V.; Egorov, M.V.; Kasimova, A.A.; Shpirt, A.M.; Shashkov, A.S.; Knirel, Y.A.; Kostryukova, E.S.; Miroshnikov, K.A. Depolymerisation of the *Klebsiella pneumoniae* Capsular Polysaccharide K21 by Klebsiella Phage K5. *Int. J. Mol. Sci.* **2023**, *24*, 17288. [CrossRef] [PubMed]
80. Gorodnichev, R.B.; Volozhantsev, N.V.; Krasilnikova, V.M.; Bodoev, I.N.; Kornienko, M.A.; Kuptsov, N.S.; Popova, A.V.; Makarenko, G.I.; Manolov, A.I.; Slukin, P.V.; et al. Novel *Klebsiella pneumoniae* K23-Specific Bacteriophages From Different Families: Similarity of Depolymerases and Their Therapeutic Potential. *Front. Microbiol.* **2021**, *12*, 669618. [CrossRef] [PubMed]
81. Magiorakos, A.-P.; Srinivasan, A.; Carey, R.B.; Carmeli, Y.; Falagas, M.E.; Giske, C.G.; Harbarth, S.; Hindler, J.F.; Kahlmeter, G.; Olsson-Liljequist, B.; et al. Multidrug-Resistant, Extensively Drug-Resistant and Pandrug-Resistant Bacteria: An International Expert Proposal for Interim Standard Definitions for Acquired Resistance. *Clin. Microbiol. Infect.* **2012**, *18*, 268–281. [CrossRef] [PubMed]
82. Vijayakumar, S.; Ramaiah, S. A Comparative Genomic Approach to Identify Determinants of Meropenem Resistance in *Klebsiella pneumoniae* Using Pan-Genome-Wide Association Analysis. *Front. Microbiol.* **2026**, *17*, 1851170. [CrossRef] [PubMed]
83. Turner, D.; Kropinski, A.M.; Adriaenssens, E.M. A Roadmap for Genome-Based Phage Taxonomy. *Viruses* **2021**, *13*, 506. [CrossRef] [PubMed]
84. Lin, T.-L.; Yang, F.-L.; Ren, C.-T.; Pan, Y.-J.; Liao, K.-S.; Tu, I.-F.; Chang, Y.-P.; Cheng, Y.-Y.; Wu, C.-Y.; Wu, S.-H.; et al. Development of *Klebsiella pneumoniae* Capsule Polysaccharide-Conjugated Vaccine Candidates Using Phage Depolymerases. *Front. Immunol.* **2022**, *13*, 843183. [CrossRef] [PubMed]
85. Dunstan, R.A.; Bamert, R.S.; Tan, K.S.; Imbulgoda, U.; Barlow, C.K.; Taiaroa, G.; Pickard, D.J.; Schittenhelm, R.B.; Dougan, G.; Short, F.L.; et al. Epitopes in the Capsular Polysaccharide and the Porin OmpK36 Receptors Are Required for Bacteriophage Infection of *Klebsiella pneumoniae*. *Cell Rep.* **2023**, *42*, 112551. [CrossRef] [PubMed]
86. Ouyang, R.; Costa, A.R.; Cassidy, C.K.; Otwinowska, A.; Williams, V.C.J.; Latka, A.; Stansfeld, P.J.; Drulis-Kawa, Z.; Briers, Y.; Pelt, D.M.; et al. High-Resolution Reconstruction of a Jumbo-Bacteriophage Infecting Capsulated Bacteria Using Hyperbranched Tail Fibers. *Nat. Commun.* **2022**, *13*, 7241. [CrossRef] [PubMed]
87. Chua, J.E.H.; Manning, P.A.; Morona, R. The *Shigella flexneri* Bacteriophage Sf6 Tailspike Protein (TSP)/Endorhamnosidase Is Related to the Bacteriophage P22 TSP and Has a Motif Common to Exo- and Endoglycanases, and C-5 Epimerases. *Microbiology* **1999**, *145*, 1649–1659. [CrossRef] [PubMed]
88. Freiberg, A.; Morona, R.; Van den Bosch, L.; Jung, C.; Behlke, J.; Carlin, N.; Seckler, R.; Baxa, U. The Tailspike Protein of Shigella Phage Sf6. A Structural Homolog of Salmonella Phage P22 Tailspike Protein without Sequence Similarity in the Beta-Helix Domain. *J. Biol. Chem.* **2003**, *278*, 1542–1548. [CrossRef] [PubMed]
89. Müller, J.J.; Barbirz, S.; Heinle, K.; Freiberg, A.; Seckler, R.; Heinemann, U. An Intersubunit Active Site between Supercoiled Parallel Beta Helices in the Trimeric Tailspike Endorhamnosidase of *Shigella flexneri* Phage Sf6. *Structure* **2008**, *16*, 766–775. [CrossRef] [PubMed]
90. Teh, M.Y.; Furevi, A.; Widmalm, G.; Morona, R. Influence of *Shigella flexneri* 2a O Antigen Acetylation on Its Bacteriophage Sf6 Receptor Activity and Bacterial Interaction with Human Cells. *J. Bacteriol.* **2020**, *202*, e00363-20. [CrossRef] [PubMed]
91. Huang, Y.; Huang, Y.; Wu, Z.; Fan, Z.; Zheng, F.; Liu, Y.; Xu, X. Characterization and Genomic Insights into Bacteriophages Kpph1 and Kpph9 against Hypervirulent Carbapenem-Resistant *Klebsiella pneumoniae*. *Virulence* **2025**, *16*, 2450462. [CrossRef] [PubMed]
92. Pan, Y.-J.; Lin, T.-L.; Chen, C.-T.; Chen, Y.-Y.; Hsieh, P.-F.; Hsu, C.-R.; Wu, M.-C.; Wang, J.-T. Genetic Analysis of Capsular Polysaccharide Synthesis Gene Clusters in 79 Capsular Types of *Klebsiella* spp. *Sci. Rep.* **2015**, *5*, 15573. [CrossRef] [PubMed]
93. Wintachai, P.; Naknaen, A.; Thammaphet, J.; Pomwised, R.; Phaonakrop, N.; Roytrakul, S.; Smith, D.R. Characterization of Extended-Spectrum-β-Lactamase Producing *Klebsiella pneumoniae* Phage KP1801 and Evaluation of Therapeutic Efficacy in Vitro and in Vivo. *Sci. Rep.* **2020**, *10*, 11803. [CrossRef] [PubMed]
94. Santiago, A.J.; Burgos-Garay, M.L.; Kartforosh, L.; Mazher, M.; Donlan, R.M. Bacteriophage Treatment of Carbapenemase-Producing *Klebsiella pneumoniae* in a Multispecies Biofilm: A Potential Biocontrol Strategy for Healthcare Facilities. *AIMS Microbiol.* **2020**, *6*, 43–63. [CrossRef] [PubMed]
95. Seed, K.D.; Dennis, J.J. Experimental Bacteriophage Therapy Increases Survival of Galleria mellonella Larvae Infected with Clinically Relevant Strains of the Burkholderia cepacia Complex. *Antimicrob. Agents Chemother.* **2009**, *53*, 2205–2208. [CrossRef] [PubMed]
96. Antoine, C.; Laforêt, F.; Blasdel, B.; Glonti, T.; Kutter, E.; Pirnay, J.P.; Mainil, J.; Delcenserie, V.; Thiry, D. Efficacy Assessment of PEV2 Phage on *Galleria mellonella* Larvae Infected with a *Pseudomonas aeruginosa* Dog Otitis Isolate. *Res. Vet. Sci.* **2021**, *136*, 598–601. [CrossRef] [PubMed]

97. Latka, A.; Lemire, S.; Grimon, D.; Dams, D.; Maciejewska, B.; Lu, T.; Drulis-Kawa, Z.; Briers, Y. Engineering the Modular Receptor-Binding Proteins of Klebsiella Phages Switches Their Capsule Serotype Specificity. *mBio* **2021**, *12*, e00455-21. [CrossRef] [PubMed]
98. Pas, C.; Latka, A.; Fieseler, L.; Briers, Y. Phage Tailspike Modularity and Horizontal Gene Transfer Reveals Specificity towards E. Coli O-Antigen Serogroups. *Virol. J.* **2023**, *20*, 174. [CrossRef] [PubMed]

**Disclaimer/Publisher's Note:** The statements, opinions and data contained in all publications are solely those of the individual author(s) and contributor(s) and not of MDPI and/or the editor(s). MDPI and/or the editor(s) disclaim responsibility for any injury to people or property resulting from any ideas, methods, instructions or products referred to in the content.